Fall 2016

Characterization of electric solid propellant pulsed microthrusters

Matthew Scott Glascock

Department:

CHARACTERIZATION OF ELECTRIC SOLID PROPELLANT PULSED MICROTHRUSTERS

by

MATTHEW SCOTT GLASCOCK

A THESIS

Presented to the Faculty of the Graduate School of the

MISSOURI UNIVERSITY OF SCIENCE AND TECHNOLOGY

In Partial Fulfillment of the Requirements for the Degree

MASTER OF SCIENCE IN AEROSPACE ENGINEERING

2016

Approved by

Joshua L. Rovey, Advisor
David W. Riggins
Henry J. Pernicka

PUBLICATION THESIS OPTION

This thesis consists of the following two articles, formatted in the style used by the Missouri University of Science and Technology:

Paper I: Pages 4-39 has been accepted by the AIAA Journal of Propulsion and Power.

Paper II: Pages 40-59 are intended for submission to the AIAA Journal of Propulsion and Power.

ABSTRACT

Electric solid propellants are an attractive option for space propulsion because they are ignited by applied electric power only. In this work, the behavior of pulsed microthruster devices utilizing such a material is investigated. These devices are similar in function and operation to the pulsed plasma thruster, which typically uses Teflon as propellant. A Faraday probe, Langmuir triple probe, residual gas analyzer, pendulum thrust stand and high speed camera are utilized as diagnostic devices. These thrusters are made in batches, of which a few devices were tested experimentally in vacuum environments. Results indicate a plume electron temperature of about 1.7 eV, with an electron density between 10^{11} and 10^{14} cm^{-3}. According to thermal equilibrium and adiabatic expansion calculations, these relatively hot electrons are mixed with ~2000 K neutral and ion species, forming a non-equilibrium gas. From time-of-flight analysis, this gas mixture plume has an effective velocity of 1500-1650 m/s on centerline. The ablated mass of this plume is 215 μg on average, of which an estimated 0.3% is ionized species while 45±11% is ablated at negligible relative speed. This late-time ablation occurs on a time scale three times that of the 0.5 ms pulse discharge, and does not contribute to the measured 0.21 mN-s impulse per pulse. Similar values have previously been measured in pulsed plasma thrusters. These observations indicate the electric solid propellant material in this configuration behaves similar to Teflon in an electrothermal pulsed plasma thruster.

ACKNOWLEDGMENTS

First and foremost, I would like to thank my advisor, Dr. Josh Rovey, without whom this work would have never taken form. Dr. Rovey has been known to occupy my desk in the late afternoon on beautiful Fridays in the spring to inquire the location of his top graduate students via email. Through this and many other interactions, he has inspired me to better myself professionally and academically. I eagerly look ahead to the future of my graduate studies with him, and will forever appreciate the time spent under his supervision. Additionally, I would like to thank the members of my committee for agreeing to serve and offering their technical knowledge and advice to me in completion of this work.

Huge thanks are due to the Missouri Space Grant Consortium, the Chancellor's Fellowship program and especially the NASA Space Technology Research Fellowship for supporting this work and my graduate career financially. Further, Digital Solid State Propulsion provided not only support via funding but also the microthrusters, essential testing hardware and help from members of its staff. Specifically, I must thank Jason Thrasher for personally helping get the testing off the ground, Shae Williams for many a fruitful discussion on the observations made, Tim Manship for assistance with the high speed camera and of course John Sousa for infinite patience and diligence in the repair of his electronic equipment. I would like to also acknowledge others who offered help on this work while asking nothing in return. The machinists of the MAE department here at Missouri S&T, John Sumpter and Warner Meeks have all been asked for much by me during the course of this work, and assisted greatly. Of course, I must thank my colleagues in the Aerospace Plasma Lab at Missouri S&T for sustaining a friendly and intellectual work atmosphere.

Finally, many thanks are due to my loving family and friends for much needed moral support in my career. Though many of you are unaware of the material of this work, it is only with your encouragement of me that it has been completed.

TABLE OF CONTENTS

LIST OF ILLUSTRATIONS

LIST OF TABLES

1. INTRODUCTION

This thesis presents work the characterization of a novel electric solid propellant operating in a pulsed microthruster configuration. This device configuration operates similar to a type of in-space electric propulsion device, the pulsed plasma thruster, which typically uses Teflon® as a propellant. Primary objectives are the formation of key observations of behavior and performance of the electric solid propellant in this configuration and key comparisons to that of the traditional propellant. A fundamental understanding of this novel propellant's behavior could be used in the future to optimize device configuration for performance, or expand the propellant's applications.

In this thesis, two papers prepared for publication in an aerospace journal are presented on this topic. The first paper details the characterization of the weakly ionized exhaust plume created during a pulse of the electric solid propellant microthruster. The second paper supplements this work with findings of propellant ablation following the primary discharge, and the negative impact this behavior has on the efficiency of the microthruster. The work in these papers offers great insight to the behavior and performance of the novel propellant, and comparisons to the propellant used typically. Preceding these papers is an introduction to the above mentioned topics, as well as the motivation driving research on this topic.

1.1. ELECTRIC SOLID PROPELLANTS

Research on Electric Solid Propellants (ESPs) has emerged in recent years due to its attractive characteristics, particularly in the field of aerospace propulsion. In basest form, ESPs are a solid rocket propellant that is only ignited when sufficient electric power is supplied to the material. Like in solid rocket propellants, this power initiates a chemical reaction in the material, which releases significant stored energy stored in the chemical bonds of the propellant constituents. Much unlike solid rocket propellants, however, once this input power is removed (or "switched" off) the chemical reaction halts and the propellant burn is completely extinguished. In modern ESPs, this cycle can then be repeated until there is no longer any propellant to be ignited. Additionally, this behavior desensitizes the propellant to accidental ignition from external sources such as

sparks, external shock or even direct flame. These characteristics give ESPs a large advantage over most energetic materials in safety and handling. Work on ESPs began in the 1990s, with the investigation of an eco-friendly air bag inflator propellant as an alternative to those containing the toxic sodium azide. A new ammonium nitrate based material was developed and the U.S. Air Force saw the potential for other applications of this propellant, namely, rocket propulsion. In short time, the first solid propellants which could be extinguished in a controlled manner, beginning with the compound "ASPEN." This material showed performance metrics similar to that of solid rocket propellants, but experienced significant problems with ignition. Thus, a modern breed of electric solid propellants was developed with higher conductivity and specific impulse. This new energetic material, the high performance electric propellant (HIPEP), is based on the inorganic hydroxyl-ammonium-nitrate (HAN). This ionic liquid serves as the oxidizer of the propellant and incites the creation of nitric acid when electric power is applied, initiating chemical breakdown. This pyroelectric behavior is fundamental to the character of the HIPEP, which is the first known energetic material to exhibit such behavior. Because these propellants respond so readily to electric power, they have also garnered attention for application in the electric spacecraft propulsion field. More specifically, these materials have been tested as propellant in the pulsed plasma thruster device.

1.2. PULSED PLASMA THRUSTER

The pulsed plasma thruster (PPT) is an in-space electric propulsion device first flown in 1964 aboard a Soviet spacecraft, marking the first ever application of electric propulsion. PPT operation begins with a high-current capacitive discharge across the exposed surface of a solid propellant, usually Teflon® (PTFE), between two electrodes. This discharge can be initiated via a number of methods, the most common being the short pulse of a spark plug or gap embedded in the cathode. The introduction of charge carriers from this pulse initiates breakdown of the electric field into a plasma arc discharge between the electrodes near the surface of the propellant. Exposure to this high-temperature plasma causes the propellant to rapidly ablate material, supplying plume constituents that may or may not then become ionized. This plasma is then accelerated to high velocities by one (or a combination) of two mechanisms. The

temperatures in such an arc discharge are sufficiently high to provide high exhaust velocities via thermal energy. This is referred to as the electrothermal acceleration. On the other hand, the electromagnetic force arising from the $j \times B$ current front in the device may also contribute to particle acceleration, leading greatly increased exhaust velocity.

The ESPs mentioned above have all been tested as propellant in a PPT, instead of PTFE, and have shown comparable performance marks (e.g. thrust, specific impulse). However, at this time it is unclear how key differences in the propellant makeup affect the current performance of ESPs in a propellant, or the potential applications for these propellants. For instance, PTFE is a solid synthetic polymer (fluorocarbon) material, where HIPEP (an ESP) is a soft solid mixture of an inorganic ionic liquid (HAN) and a similar synthetic polymer, polyvinyl alcohol. PTFE seals out atmospheric moisture extremely well, while HIPEP is very hygroscopic. The ESP is also quite conductive, but PTFE is an excellent electrical insulator.

1.3. OBJECTIVES

Because ESP materials are new to the electric propulsion research field, it is desired that a clear comparison is drawn between these materials and the current state-of-the-art propellants. In the case of the PPT, the behavior of the ESP material should be compared to that of PTFE. Thus, the primary objectives of this work are to first describe the operation of a PPT-like device using an ESP in as much detail as possible, then discuss the observed similarities or differences in this operation to that of traditional PPTs using PTFE as propellant. The first paper presented in this thesis focuses on the experimental characterization of the ESP device. The key parameters of the plume created by this device like the electron temperature and density, ionization fraction, and effective velocity are examined. Further, the propellant mass ablated by the device per shot and the composition of this mass (i.e. the plume) are investigated. These properties are then compared to those previously measured in PTFE PPT research, which has been extensively detailed in the literature. The second paper focuses specifically on the ablation process of the ESP material. Measurements of the ablation mass and measured impulse per pulse are compared to those of exhaust velocity. High speed photography is also introduced to provide qualitative observations of this propellant ablation. Again, the findings in the work of the second paper are compared to those of traditional PPTs.

PAPER

I. PLUME CHARACTERIZATION OF ELECTRIC SOLID PROPELLANT PULSED MICROTHRUSTERS

Matthew S. Glascock and Joshua L. Rovey,
Missouri University of Science and Technology, Rolla, Missouri, 65409
and
Shae Williams and Jason Thrasher,
Digital Solid State Propulsion, Reno, Nevada, 89511

ABSTRACT

Electric solid propellants are an attractive option for propulsion because they are ignited only by an applied electric current. This leads to capabilities such as on-demand throttling and re-ignition in chemical combustion operation, and lends itself to application in electric propulsion. In this work, the plasma plume created by electric solid propellant pulsed microthrusters is investigated using a nude Faraday probe, a triple Langmuir probe, and residual gas analysis. The thrusters were tested at a vacuum level of 2×10^{-5} Torr. Results indicate an average plume electron temperature of 1.7 eV and a density of 10^{11} to 10^{14} cm^{-3}. Time-of-flight analysis indicates an exhaust velocity of 1500-1650 m/s on centerline. Additionally, ionization fraction is estimated to be 0.3% for an ablation mass bit of 215 μg on average. Thermal equilibrium and adiabatic expansion calculations suggest a non-equilibrium gas with high-temperature electrons and lower temperature neutral and ion species. Results indicate the pulsed microthruster operates similar to a coaxial pulsed plasma thruster, and is dominated by electrothermal effects.

NOMENCLATURE

A_n	=	probe collection area of probe n; n = 1, 2, 3
h	=	Planck constant
I_n	=	current flow in probe n
I_p	=	probe current
j	=	current density
k	=	Boltzmann constant
MW	=	molecular weight
m_e	=	electron mass
m_i	=	mass of ion species i
n_e	=	electron number density
P_n	=	probe label
p	=	pressure
Q_i	=	ion charge
$Q_{int}^{Z, Z+}$	=	internal partition function
$\Re$	=	universal gas constant
T	=	temperature
T_c	=	chamber temperature
T_e	=	electron and exhaust temperature
t_d	=	time duration of microthruster discharge pulse
V_{d2}	=	voltage difference between probe 1 and probe 2
V_{d3}	=	bias voltage between probe 1 and probe 3
r_p	=	probe tip radius
s	=	probe tip separation distance
λ_D	=	Debye length
d_s	=	plasma sheath diameter
λ_{ie}	=	charged particle collision mean-free path
$V_{ex, ue}$	=	exhaust velocity
V_f	=	floating potential, with respect to ground
V_n	=	voltage of probe n, with respect to space potential

V_p	=	space potential
γ	=	ratio of specific heats
φ	=	ionization fraction
θ_i	=	ionization potential

1. INTRODUCTION

Electric solid propellants (ESP's) are an emerging topic of research with major implications in the field of propulsion from the micro to macro scale [1-3]. These propellants offer exciting capabilities for controlling solid chemical rocket motors previously unheard of for typical energetic materials. When electric power at the proper current and voltage levels is applied to an ESP, the solid propellant ignites and continues to exothermically decompose until that power is removed. This process can be repeated until the solid propellant is entirely consumed. Further, the burn rate of the propellant can be throttled by altering the electrical power applied. This method of operation is not possible with traditional solid rocket propellants and energetics, and greatly expands the potential applications for solid rocket motors that are fit with an ESP. Additionally, ESPs are insensitive to accidental ignition by spark, impact or even open flame. This is a huge advantage over most energetics in safety considerations and ease of use.

The development of ESPs began in the mid-late 90's with the investigation of a "green" automobile air bag inflator propellant (ABIP). This ammonium nitrate based material quickly garnered attention from the U.S. Air Force for other applications, including a patented formulation [4] for rocket propulsion application. Soon after, the first controlled extinguishable solid propellants were developed, the first of which was referred to as "ASPEN." This development process began adding ingredients to the ammonium nitrate based propellant to lower the melting point and increase the electrical conductivity during chemical combustion. Performance metrics of the ASPEN propellant were comparable to typical marks for solid rocket motors, but experienced major problems with initial ignition. Addressing these problems led to the development of a more advanced formula to achieve higher specific impulse and conductivity of the propellant. This higher performance electric propellant (HIPEP) is a hydroxyl ammonium nitrate (HAN) based energetic material. In this formulation, the ionic liquid oxidizer HAN exhibits a pyroelectric behavior; the application of electric power to this material incites the creation of nitric acid, triggering ignition of the formulation. This behavior has been previously observed in organic materials, but none of which are known to be energetic.

Electric solid propellants have also been tested for application in electric propulsion. All of the aforementioned ESP's have been tested as alternative fuel/propellant for the ablation fed pulsed plasma thruster and have shown performance marks comparable to that of the traditional Teflon propellant [3]. The Pulsed Plasma Thruster [5, 6] (PPT) is a type of in-space electric propulsion system first flown in November of 1964 aboard the Soviet spacecraft Zond 2, marking the first application of electric propulsion on a spacecraft. Modern PPT's are primarily used for stationkeeping needs [7-9], attitude control [10-12], and other secondary propulsion system duties [13]. These thrusters have received considerable attention in the propulsion community due to the relative simplicity of the supporting technology and their ability to reliably generate small impulse bits.

Operation of the ablation-fed PPT begins with a high-current discharge between electrodes across the exposed surface of a solid propellant, typically Teflon® (PTFE). Burton and Turchi [5] illustrate two distinct operating modes for this discharge: the ablation arc or the propagating mode. Typically the mode is influenced by whether the PPT is in a breech-fed or a side-fed [14] configuration. Breech-fed PPT's, such as the LES-6 typically do not exhibit mass ablation rates great enough to sustain a stable arc at the surface of the propellant, thus the current distribution propagates downstream, reducing the ablation rate [15]. In side-fed devices, the heat transfer from the arc discharge to the propellant is sufficient to provide new particles at a rate to sustain the arc near the propellant surface. In addition to these arc operating modes, PPT's are typically classified by geometry into rectangular and coaxial configurations. The LES 8/9 and the University of Illinois PPT-3/PPT-4 designs are examples of a rectangular and coaxial PPT configuration, respectively. Additionally, the LES 8/9 is a breech-fed device [9] that exhibits a propagating discharge mode of operation, while the PPT-3/PPT-4 device is a side-fed PPT with an ablation arc operation [5, 16]. These two designs are also examples of the differing acceleration mechanisms often observed in PPT operation. The LES 8/9 has a plume that is ionized by the main discharge (~10% ionization fraction) and accelerated by the electromagnetic force arising from the $j \times B$ current front that propagates along with the ablated mass [17]. These high-energy, high-velocity particles contribute 15% (or more) of the kinetic energy of the exhaust gas despite the much lower

mass compared to the rest of the plume, which remains neutral. On the other hand, in the PPT-3/PPT-4 device the acceleration of the ablated mass is dominated by electrothermal effects [16]. The temperature arising from the arc discharge is sufficiently high to provide exhaust velocities comparable to or even exceeding that of chemical thrusters. These temperatures are typically limited by radiation and other dissipative processes to a few eV, but the high temperature neutrals provide nearly the entirety of the kinetic energy in the exhaust [18]. Additionally, both thrusters (and most PPTs in general) have shown evidence of lost mass after the completion of the discharge pulse in the form of low velocity neutrals and even macroparticles that contribute little to nothing by way of performance, though the mass fraction of this "late-time ablation" is not well characterized [19].

This paper focuses on the exhaust plume of a PPT operating with an electric solid propellant. Results from ion current density, electron temperature, and time-averaged plume species composition are coupled with thermodynamic equilibrium calculations and adiabatic expansion to show that the PPT operates in an electrothermal mode. Additionally impulse bit measurements are presented from thrust stand testing. The experimental apparatus is described in Section 2, and the Results and Analysis are given in Section 3 and 4, respectively. Conclusions from the work are described in Section 5.

2. EXPERIMENTAL APPARATUS

The PPT microthrusters are described, along with the ESP and power processing unit. Then the facilities in which the microthrusters are operated are described, followed by the diagnostics used to characterize the plume.

2.1. MICROTHRUSTERS AND POWER PROCESSING UNIT

The microthrusters used in this work are an initial configuration, and a main goal of this work is to help guide design of a higher performance variant. The microthrusters have a coaxial geometry as shown in Figure 2.1. The outer electrode is a 3.2 mm diameter aluminum tube and the concentric inner electrode is a 1.2 mm diameter molybdenum rod. The total length of the microthruster is about 2.5 cm, with the propellant grain measuring roughly half of that length. The molybdenum inner electrode is also coated with polymer insulation (shellac) with a nominal thickness of 0.03 mm. The ESP has an annular shape and fills the space between the inner and outer electrodes. By applying a relatively low voltage discharge from a capacitor bank (300 V) for a short duration pulse (about 0.5 ms) a small mass of the ESP is ablated and expelled from the thruster. Performance testing indicates that the impulse bit is 200-500 μN-s per pulse, with a specific impulse estimated on the order of 200 seconds. In general, these microthrusters have an operation lifetime of around 200 pulses.

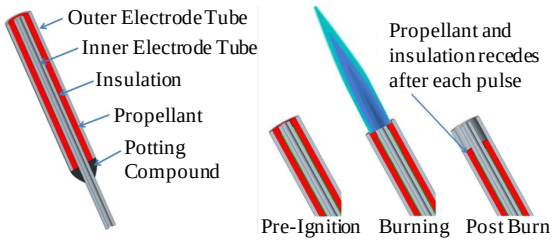

Figure 2.1: CAD Model illustrating composition and operation of the ESP microthruster.

The ESP is a hydroxyl ammonium nitrate (HAN)-based solution solid manufactured using benign processes and “green” ingredients, mixed in standard chemical glassware and cured conveniently at warm room temperatures (35°C/95°F). It

has a chemical composition of HAN oxidizer (an inorganic ionic liquid) and polyvinyl alcohol (PVA) fuel binder, which make up 95% of the propellant, as shown in Table 2.1. The ESP is initially a liquid and injected by syringe into the discharge gap of the microthruster. It is then cured to form a soft solid with the appearance and texture of a soft pencil eraser. It is safe to handle and classified under DOT as a 1.4S explosive, making this ESP much more convenient to transport and work with than conventional solid rocket propellants.

Table 2.1: Nominal composition of the High Performance Electric Propellant tested in the microthrusters.

Chemical Name	Chemical Formula	Percentage by mass	Molecular Mass, g/mol
Hydroxyl Ammonium Nitrate (HAN)	$(NH_3OH)^+ NO_3^-$	75%	96
Polyvinyl Alcohol (PVA)	$CH_2CH(OH)$	20%	44
Ammonium Nitrate (AN)	NH_4NO_3	5%	80

There are some key differences between the ESP and traditional Teflon (PTFE) PPT propellant. PTFE is a fluorocarbon solid, while the ESP is a soft-solid mixture with composition given in Table 2.1. In a typical PPT, the PTFE is an electrical insulator between the electrodes. The conductivity of the ESP in this work is comparable to "highly conductive" ionic liquids which have been selected as candidates for use in dye-sensitized solar cells [20]. With the ESP propellant the pulsed electric current can be conducted through the ESP, potentially initiating thermoelectric decomposition and creation of intermediates in the propellant. With PTFE an arc discharge is created near the surface of the solid PTFE, ablating the propellant via heat transfer. Additionally, in a conventional PPT, the propellant is fed into the thruster such that the arc discharge always occurs at the same physical location with respect to the thruster exit plane. With the ESP microthrusters the propellant face recedes from the exit plane over time as the

propellant is burned away. It is currently unclear how these propellant differences affect the operation and performance of a PPT using the ESP as a propellant.

The power processing unit (PPU) used to operate the microthrusters is a custom in-house pulsed power supply. This PPU is primarily a bank of capacitors with a nominal rating of 900 μF. This bank is charged to 300 V with a small input power (5 V at < 1A). Once charged, the stored energy (about 40 J) is then rapidly discharged directly into the thruster electrodes, an event which typically lasts about 500 μs. This mode of operation was chosen as it was shown to increase the total impulse delivered over the thruster lifetime. Additionally, the voltage level of 300 V was chosen to keep the impulse bit per pulse around 500 μN-s. This PPU is vacuum-compatible and is mounted a few inches from the thruster during testing; the PPU is then remotely controlled via serial communication.

2.2. VACUUM FACILITIES

2.2.1. Missouri S&T Aerospace Plasma Lab. The microthrusters were tested in the large (1.8 m dia., 3 m lg.) space and high altitude vacuum facility at the Aerospace Plasma Laboratory of Missouri S&T. This facility uses four 89 cm diameter oil vapor diffusion pumps backed by an Edwards EH 4200 roots-blower pump and a Tokunda KP-7500BG rotary-vane pump. Standard operation for this work was two oil vapor diffusion pumps active which gives the facility a nominal base pressure of 2×10^{-5} Torr. The interior of the facility is equipped with a two-axis translation table system with a minimum step size of 2.6 μm that is controllable remotely to allow for the measurements made at varying locations.

2.2.2. Digital Solid State Propulsion (DSSP) Vacuum Facility. Microthrusters were also tested in the large vacuum facility at DSSP. This facility uses a single Varian VHS-250 oil vapor diffusion pump and an Alcatel ADS501 model rotary-vane, roots-blower pump combination for roughing of the chamber. Standard operation for this work was with the oil vapor diffusion pump active, yielding a nominal base pressure of 5×10^{-4} Torr. The interior of the facility is equipped with an optical table for mounting of hardware and diagnostics.

2.3. DIAGNOSTICS

Characterization of the plasma plume created during a pulse is generally the first step of analyzing a PPT system, and the primary focus of this work. Plume velocity distribution, plasma density and temperature, and current density are useful in analyzing performance of a PPT. Plasma plume characterization of the microthruster has been conducted at Missouri S&T and DSSP. A number of prevalent PPT plume diagnostics were prepared and used for the analysis of the microthruster. Faraday probe measurements for bulk plasma current [21, 22] and a Langmuir triple probe [23-26] to determine plasma densities and temperatures were employed as plasma diagnostic tools. Additionally, a residual gas analyzer [27] and mass balance were used to investigate the composition of the plume and the ablated mass per pulse. Finally, a thrust stand was used to measure the impulse bit of microthrusters.

2.3.1. Faraday Probe. The nude Faraday Probe (FP) is used to measure the ion current density in the plume of an electric propulsion device, be it an electrostatic device such as a Hall Effect thruster, or a pulsed device such as the PPT. The nude Faraday probe has a sensitivity to vacuum facility effects and elevated backpressures. Walker et al. [22] reported maxima of -20% and +20% difference in FP current density measurements at angles of 20° and 60° off-centerline between measurements made at 1.2×10^{-5} and 4.2×10^{-6} Torr. On centerline, this value is less than 10%. In this work, the nominal base pressure is on the order of 10^{-5} Torr, indicating the error due to this effect is about 10% of the peak measured current density, found on centerline. Due to the low measured ablation mass, it is expected that the local pressure at the face of the probe will not exceed this order of 10^{-5} Torr. As signal noise was less than 1% peak value, this backpressure sensitivity is the dominant source of error in these measurements. Thus, the overall uncertainty in FP measurements is taken to be 10%. The Faraday probe used in this work is shown in Figure 2.2.

The probe and guard ring are biased to a negative voltage (in this work, -30 V relative to ground) to repel stray electrons and encourage the collection of ions. The center collector is then connected to a measurement circuit similar to that of a traditional planar Langmuir probe. Monitoring the current draw through the collector of the Faraday probe provides the ion current density of the plume.

Figure 2.2: Faraday Probe integrated into large vacuum chamber diagnostic probe arm.

The collector is 2.54 cm (1") in diameter, giving it a circular (planar) collection area of about 5 cm^2. Because the size of this probe is quite large relative to the microthruster and the estimated size of the plasma plume created, it is assumed that the probe will collect a large majority of the ions present in the plume when positioned near (~5 cm) the thruster exhaust and aligned with the axis of the microthruster. The Faraday probe was positioned on R-Z translation stages in the vacuum test facility, allowing it to make measurements of the ion current density at selected axial and radial locations.

2.3.2. Langmuir Triple Probe. The Langmuir Triple Probe (LTP) is used to measure electron density and electron temperature without requiring a voltage sweep. This makes the LTP well suited to operation in pulsed environments, and a common diagnostic for the pulsed plasma thruster [25, 26]. Tungsten wire of 0.5 mm diameter was inserted into three bores of a quad-bore alumina tube of 10 mm diameter, creating the three isolated probe tips of 5.0 mm in length, separated by 1.5 mm. The remaining bore is plugged with a ceramic adhesive. On the other end of the probe, the tungsten wires connect to individual standard RF cables inside a grounded enclosure.

For cylindrical geometry Langmuir probes, there are five base assumptions in the probe theory to consider. The first two concern electrical properties: (1) the measured probe currents are small relative to the discharge current and (2) the electrons in the plasma are governed by a Maxwellian energy distribution. The first criterion is readily met as the probe current, I_3 has peak values of a few Amps at most, compared to the discharge current peak of >1000 A. Electron-electron collision timescale for plasma with density 10^{12} cm^{-3} and temperature 1.7 eV is on the order of 10^{-8} s, while the thruster

discharge lasts about 5×10^{-4} s. This implies that the number of electron collisions during a pulse is sufficient to create an equilibrium Maxwellian distribution. The final three assumptions of Langmuir probe theory concern the physical size of the probe. Specifically, (1) the probe radius (r_p) must be much greater in size than the characteristic shielding (Debye) length of the plasma, λ_D, (2) probe separation distance (s) must be much larger than the Debye sheath (a positively charged plasma layer several Debye lengths thick) diameter, d_s, (3) the ratio of the mean-free path, λ_{ie}, to the probe radius (i.e. the Knudsen Number) must be greater than 1. Table 2.2 details these parameters for the region of interest for this work. It can be seen that the conditions shown here encapsulate the operating regime of this triple probe, as the previous criteria are met in all cases. However, sheath interference would be likely at electron densities lower than 10^{11} cm^{-3} and the probe radius is too large for densities and temperatures greater than the maximums in Table 2.2. Additionally, the LTP must be small compared to the characteristic length of the plasma such that the density distribution is relatively uniform across all three probe tips. Figure 2.3 shows the size and location of the LTP relative to the microthruster and a 60° divergence half-angle plume, roughly to scale. Here it is seen that the characteristic length scale (i.e. plume diameter, ~9 cm) of the plasma is about ten times the size of the probe diameter (1 cm). However, the density distribution is not uniform across the full characteristic diameter of the plume. From faraday probe measurements it is seen that the current density varies from 250-275 mA/cm^2 (~10%) over a 1 cm distance. Thus, we assume the plume is uniform to within 10% across the probe diameter.

Table 2.2: Critical parameters for the Langmuir triple probe operating regime.

Plume Conditions		Triple Probe Parameters		
		r_p/λ_D	s/d_s	λ_{ie}/r_p
$n_e = 10^{11}$ cm^{-3}	T_e = 1 eV	11.3	3.8	128
$n_e = 10^{11}$ cm^{-3}	T_e = 5 eV	5.0	8.4	3208
$n_e = 10^{12}$ cm^{-3}	T_e = 1 eV	35.6	11.9	12.8
$n_e = 10^{12}$ cm^{-3}	T_e = 5 eV	15.9	26.6	321
$n_e = 10^{13}$ cm^{-3}	T_e = 1 eV	113	37.6	1.3
$n_e = 10^{13}$ cm^{-3}	T_e = 5 eV	50.4	84.1	32.1
$n_e = 10^{14}$ cm^{-3}	T_e = 5 eV	159	266	3.2

In this work, the triple probe was operated in what is referred to as "voltage-mode," wherein (as in Figure 2.4) three identical probes are inserted into the plasma. All three probes are floating with respect to ground (V_f), and a bias voltage difference, V_{d3}, is applied externally to two of the probes via a battery. In this work, V_{d3} was selected as a nominal 27 V, supplied via three 9V batteries in series.

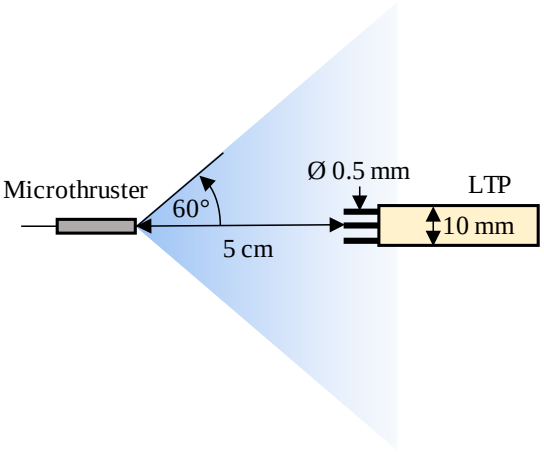

Figure 2.3: Illustration of Langmuir triple probe physical size and location relative to plume.

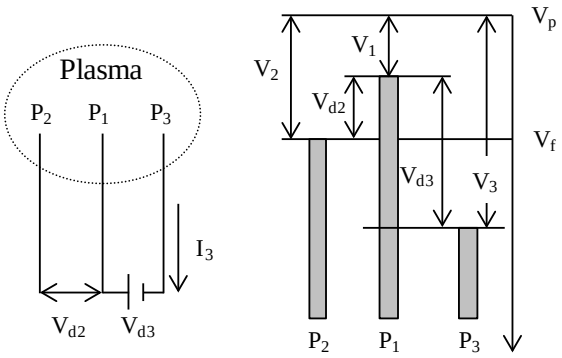

Figure 2.4: Electrical schematic and illustration of the triple Langmuir probe in voltage-mode.

During a pulse, the voltage difference V_{d2} is measured via a differential voltage probe and the probe current, I_3, is measured via a current monitor. The high voltage differential probe is less susceptible to signal noise than digitally subtracting signals on an oscilloscope, or a differential operational amplifier [25, 26]. However, the high

impedance of the differential probe limits the probe measurement circuit rise time to a minimum of 70 ns. This rise time is negligible compared to the plasma timescale, which is greater than 100 μs. These measurements are displayed as a function of time during testing on a 4-channel oscilloscope. Through the Langmuir Triple Probe theory from Chen and Sekiguchi [23, 24], outlined below, these measurements $V_{d2}(t)$ and $I_3(t)$ can be used to directly calculate the plasma electron temperature, $T_e(t)$, and the plasma density, $n_e(t)$ via equations (1) and (2) below.

$$\frac{1-\exp\left(-\frac{V_{d2}}{T_e}\right)}{1-\exp\left(-\frac{V_{d3}}{T_e}\right)}=\frac{1}{2} \tag{1}$$

$$n_e=\frac{m_i^{\frac{1}{2}}\left(\frac{I_3}{A_3}\right)1.05\times10^9}{(T_e)^{\frac{1}{2}}\left(\exp\left(\frac{V_{d2}}{T_e}\right)-1\right)} \tag{2}$$

In Eqn. 1 and 2, T_e is the electron temperature of the plasma in eV, m_i is the plume mixture mass number, I_3 the measured probe current in μA, A_3 the individual probe collection area in mm^2 and n_e is the plasma density measured in cm^{-3}. In the equations above, the applied voltage difference V_{d3} is assumed constant during each pulse; testing found that the current draw on the batteries supplying this voltage was negligible and thus a valid assumption. Additionally, the density equation requires a plasma species mass. In this work, the results from a residual gas analysis were used to estimate the plume mixture molecular mass.

2.3.3. Residual Gas Analyzer and Mass Balance. Plume species composition is estimated from measurements using a residual gas analyzer. The residual gas analyzer used for this work was an Extorr XT100 model, which is a quadrupole RGA with included Pirani gauge and hot cathode ion gauge. This model's resolution is adjustable based on the selected mass range (max width 1-100 amu), but is greater than 0.5 amu at 10% peak height; the sensitivity is 5×10^{-4} A/Torr into the detector and the device has a minimum detectable partial pressure of 10^{-11} Torr. The thruster mass before and after

testing is measured using a mass balance. The mass balance has a resolution of 1 mg, with noise on the order of that resolution.

2.3.4. Thrust Stand. The existing thrust stand previously built in-house by DSSP for performance testing of the microthrusters was used in this work. The design is a pendulum using spring steel as a dampening method. The microthruster is mounted to a fixture suspended from an aluminum frame by two pieces of 2.5 cm wide spring steel to ensure minimal cross-axis movement. During each thruster discharge, the displacement of the fixture is measured by a laser displacement sensor with a resolution of 5 μm. This corresponds to a resolution in thrust measurement of about 1 mN for typical pendulum fixture mass. The maximum expected uncertainty of the thrust stand is $\pm$10% based on error analysis in the laser and chamber back pressure. In the current configuration, the thrust stand can measure the impulse-per-pulse (or impulse bit, I_{bit}) of the microthruster within a range of 0.025 mN-s to 5 mN-s.

3. RESULTS

Experimental results from the mass balance, thrust stand, Faraday probe, triple Langmuir probe and the residual gas analyzer are presented. The mass bit, impulse bit, plume current density, plume plasma properties, and plume species composition are presented.

3.1. AVERAGE MASS BIT

Table 3.1 details the results of the mass balance measurements of fourteen selected microthrusters tested during this work. These thrusters are all at (or nearly at) the observed end-of-life. The analysis in this work focuses on the lifetime averaged behavior of the microthrusters. Average ablated mass per pulse (the mass bit) is calculated by subtracting the final from initial mass and dividing by the number of pulses. Overall, the average mass bit is 215.4 μg. This result is on the order of typical values for a PTFE PPT, which is usually between 10 and 100 μg, though it is noticeably greater. Further, in comparing the energy specific ablation mass of these devices, we find that the ESP microthruster (5.4 μg/J) falls right in line with PTFE PPTs (1.5-10 μg/J). However, examination of the mass bit per ablation area shows that the ESP microthruster (~790 $\mu g/cm^2$) is more than an order above that of typical PPTs, which fall in the range of 1-50 $\mu g/cm^2$. This is due to the comparable discharge energy and ablation mass, but a very small ablation area relative to PTFE PPTs [5].

3.2. IMPULSE BIT

Thrust testing was conducted at DSSP. A primary focus of this thrust testing was to determine the impulse bit per pulse of the microthrusters. Figure 3.1 shows these results over the pulse lifetime of four different microthrusters from various batches. The first three (RR43A08, RR50A14 and RR51A10) were tested in the DSSP vacuum facility equipped with the triple Langmuir probe diagnostic. The final thruster (RR50A20) was not interrogated with the Langmuir probe. From the data shown in Figure 3.1, the impulse bit is between 0.15-0.27 mN-s with trends that vary from thruster to thruster, as well as pulse-to-pulse. RR50A20 has an average impulse bit of 0.257 mN-s, standard deviation of 0.02 mN-s and *increases* by about 40% over its lifetime.

Table 3.1: Average ablation mass bit data for the selected microthrusters.

Serial no.	Pulses	Initial Mass (mg)	Final Mass (mg)	Average Mass Bit (μg)
OD01A09	200	639	549	450.0
OD01A12	222	647	590	256.8
OD01A13	206	642	588	262.1
OD01A14	155	636	545	587.1
OD01A17	280	643	611	114.3
OD02A06	150	637	603	226.7
OD02A10	150	625	613	80.0
RR43A08	121	641	631	82.6
RR50A14	143	658	639	132.9
RR50A20	153	661	637	156.9
RR51A03	150	661	614	313.3
RR51A06	150	642	623	126.7
RR51A10	161	641	624	105.6
RR52A10	150	665	647	120.0
			Mean:	215.4

The remaining two microthrusters, RR43A08 and RR50A14 have impulse bit averages of 0.189 and 0.199 mN-s, respectively, with relatively constant trends but wide standard deviations (0.08 and 0.05 mN-s). The average impulse bit across the four microthrusters was found to be 0.210 mN-s. These variations are not attributed to measurement error, but rather to real changes in thruster performance from pulse to pulse and thruster to thruster, the exact cause for which is not yet known.

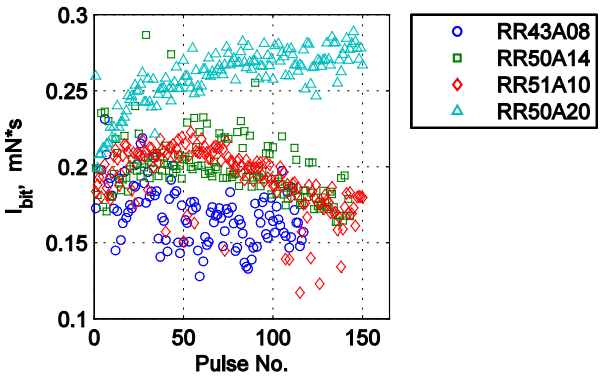

Figure 3.1: Measured impulse bit for four different microthrusters.

3.3. FARADAY PROBE RESULTS

Figure 3.2 shows typical traces of the ion current density as a function of time as measured by the nude Faraday probe at the multiple downstream locations along the centerline of thruster OD01A09. In all time-resolved measurement figures, the zero time location is aligned with the rising edge of the measured thruster discharge current at 1 A, which marks the beginning of the thruster discharge. All of the peak values were measured between 20 and 50 μs after the thruster discharge, which agrees with the time-of-flight measurements in Section 4. The greatest ion current density is at the 5 cm location, closest to the thruster exit, which peaks at about 273 mA/cm^2. The data from these traces are later used to calculate the total charge collected and determine the ionization fraction of the microthruster plume.

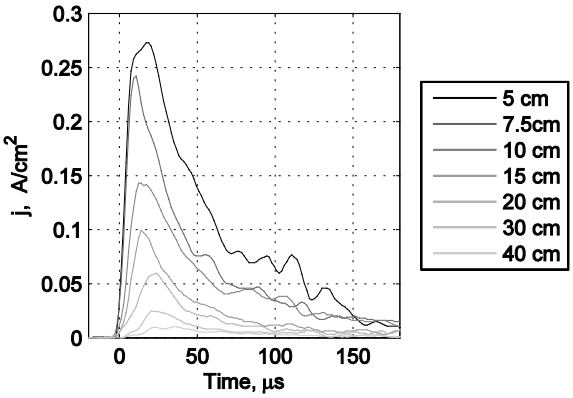

Figure 3.2: Ion current density as measured by the Faraday probe at multiple downstream locations on the thruster centerline.

Moving further from the thruster exit, the ion current density decreases by < 10% (242 mA/cm^2) at the 7.5 cm location, but quickly decreases further downstream to about 50% of that peak at 10 cm and then to about 35% at 15 cm. Further, the far-field ion current measurement at 40 cm downstream is less than 5% of that peak value (~10 mA/cm^2). Additional measurements were made with the Faraday Probe at radial locations centered at 5 cm downstream and made on-centerline and 5, 10, and 15 cm off-centerline. These results showed similar trends with the peak current density on-centerline and decreasing by about 50% at 5 cm off-centerline and more than an order of magnitude at 10 cm with the measurement decreasing to negligible levels at 15 cm off-

centerline. Marked by black dots on Figure 3.3 are the spatial locations of the Faraday probe measurements. Overlaid on this figure are contours of the peak current density as measured by the Faraday probe at these locations.

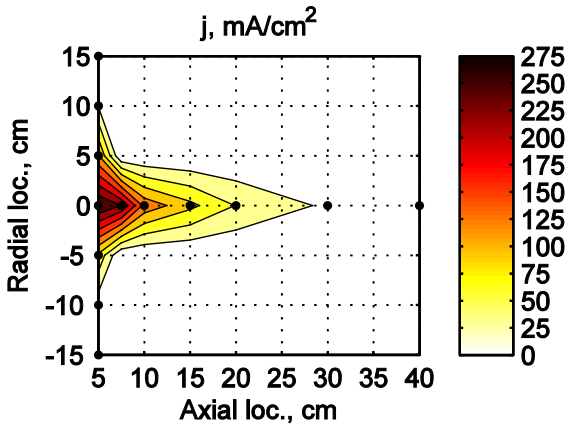

Figure 3.3: Peak current density contours, as measured by the Faraday probe at the locations marked with dots.

3.4. LANGMUIR TRIPLE PROBE RESULTS

The triple Langmuir probe provides measurements of electron temperature (T_e) and density (n_e) as a function of time for each pulse of a microthruster, taken at 5 cm downstream of the thruster on centerline. Figure 3.4 below shows typical traces of $T_e(t)$ and $n_e(t)$ typical as measured by the triple Langmuir probe for a single pulse. These results are obtained by numerical filtering of the probe current and voltage differential measurements and solution of equations (1) and (2). As seen in the figures, both the T_e and n_e measurements peak between 20 and 25 μs after the beginning of the thruster discharge. At this point, the electron temperature peaks at 1.2 eV and quickly recedes to 0.5 eV by 100 μs and then slowly increases again to about 75% peak value until quickly dropping to zero at around 400 μs. This increase at ~200 μs is not fully understood. It could be a secondary interaction of high relative energy electrons with the probe while the colder ions are still present in the vicinity of the probe. Due to this observation, the authors have chosen to report both the peak and time-averaged electron temperature values. The electron density trace peaks at a maximum value of 6.9×10^{11} cm^{-3} and

decreases constantly for about 325 μs. At ~350 μs the electron density measurement drops off to near-zero values.

For the probe parameters in Table 2.2, the expected accuracy of the triple probe measurements is within ~20% for electron temperature, and 40-60% in density [28]. The dominant source of measurement error in the triple Langmuir probe data is the significant signal noise attributed to the high-impedance measurement of V_{d2}. This bit error is on the order of $\pm$25% of peak value (~0.3 eV) in electron temperature measurement, and about 10% peak value in density measurements. The effects of other sources of error have been deemed negligible relative to the above values. Ion current models for the $5 \leq r_p/\lambda_D \leq 100$ are optimal, with only a slight error for higher ratios [23]. Plasma sheath interaction at the probe tips is unlikely because the tip separation distance is greater than the sheath diameter for the region of interest. The effect of a magnetic field on the ion current collection can be assumed negligible, as there are no applied fields, and the induced field is of negligible strength. Similarly, ion collisions are not expected to greatly influence the ion current measurements for the condition $\lambda_{ie}/r_p > 200/(r_p/\lambda_D)$, which is met for most cases as shown in Table 2.2. Thus we estimate that the maximum uncertainty in electron temperature measurements is 25% and the maximum uncertainty in the electron density measurements is 60%. These values are typical when investigating the plumes of magneto-plasma-dynamic thruster and PTFE PPT plumes [25, 28].

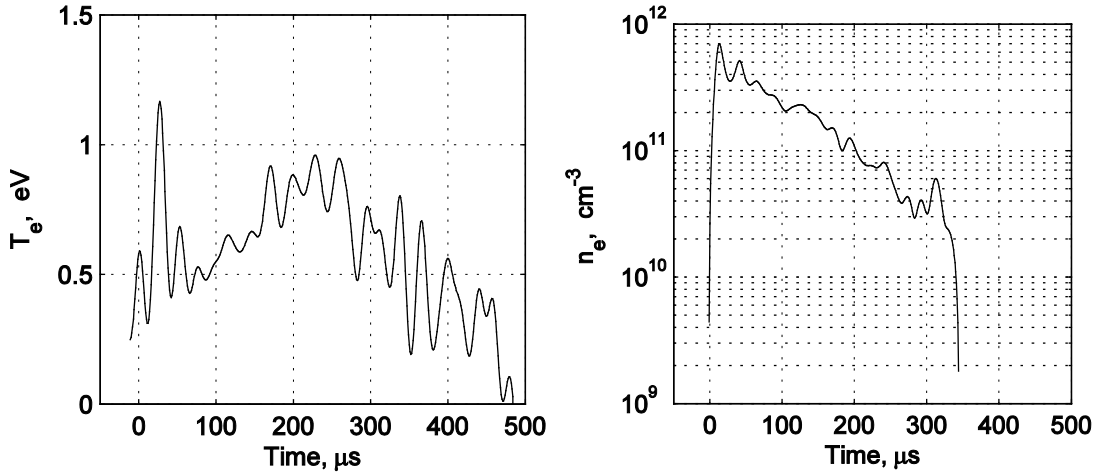

Figure 3.4: Typical trace for the electron temperature and electron density of the thruster plume as measured by the triple Langmuir probe.

Also of particular interest in this work are the observable trends in the electron temperature and density of the microthruster over its 150-200 pulse lifetime. Figure 3.5 below shows the trends of peak electron temperature and density for the lifetime of microthruster OD02A10. Peak electron temperature varies from 2 to just below 4 eV, with a generally decreasing trend for the first 40 pulses. Between 50-150 pulses, the peak electron temperature is consistently between 1 and 2 eV. Additionally, peak electron density varies from 10^{11} cm^{-3} to 10^{13} cm^{-3}. However, 80% of the peak electron density measurements lie in the 0.5×10^{12} to 1.5×10^{12} cm^{-3} range, with the average ~9.2×10^{11} cm^{-3}, which is four or more orders of magnitude lower than a typical PTFE PPT [5, 25].

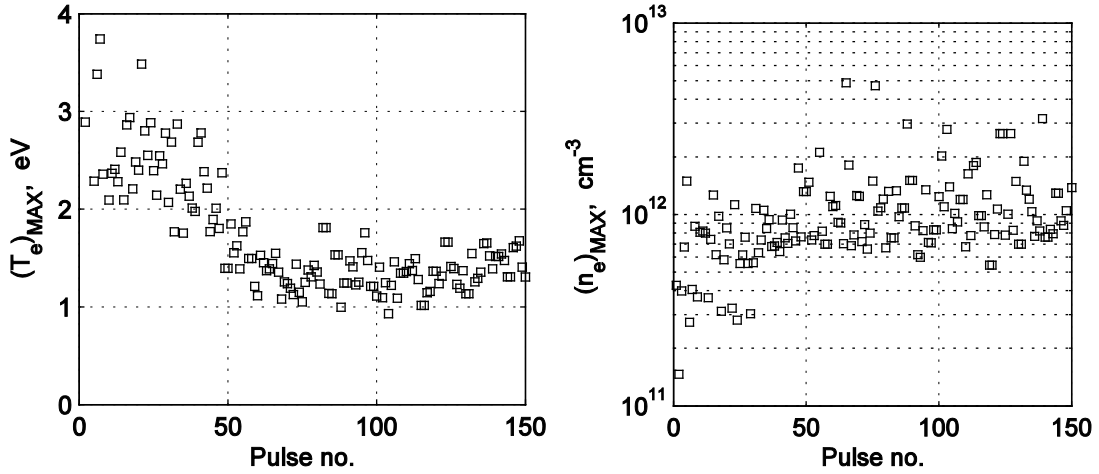

Figure 3.5: Lifetime trends observed for peak electron temperature and peak electron density of the thruster plume as measured by the triple Langmuir probe.

Further, the time-averaged electron temperature, $\langle T_e \rangle$, and electron density, $\langle n_e \rangle$ for each pulse over the duration of the pulse is obtained from equations (3) and (4) below for each pulse. The pulse duration (t_d) is determined by finding the time index of the minimum value above a tolerance (0.1 eV for T_e, 10^5 cm^{-3} for n_e), marking the end of the pulse. This value is then determined as the pulse duration, as the zero time marks the beginning of the pulse.

Figure 3.6 below shows the results of these calculations for the same microthruster (OD02A10) as shown in Figure 3.5. Time-average electron temperature calculations have a standard deviation of 0.7 eV, and roughly 65% of the calculations

falling between 0.5 and 1 eV. These results are consistent with the values and trends observed in the peak temperature measurements, with the maximum values (2-3 eV) occurring in early lifetime and decreasing sharply (<1 eV) from pulse 1 to 50. The time-average electron density is similarly consistent with the average at about 1.3×10^{11} cm^{-3}, and about 85% of the measurements just greater than 10^{11} cm^{-3}.

$$\langle T_e \rangle = \frac{1}{t_d}\int_0^{t_d} T_e(t)\,dt \tag{3}$$

$$\langle n_e \rangle = \frac{1}{t_d}\int_0^{t_d} n_e(t)\,dt \tag{4}$$

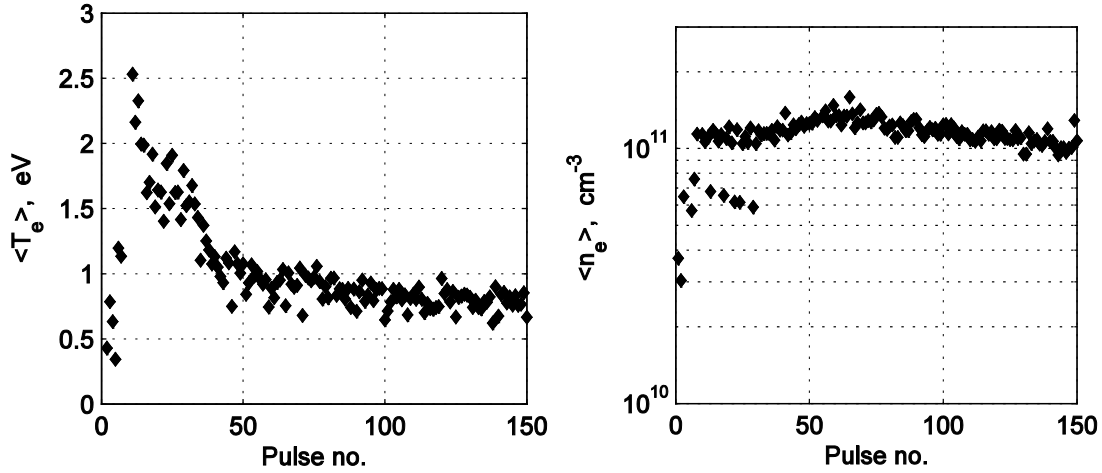

Figure 3.6: Lifetime trends observed for time-average electron temperature and time-average electron density of the thruster plume as measured by the triple Langmuir probe.

The above results for the peak electron temperature and density were tabulated for a number of thrusters tested and interrogated using the Langmuir triple probe. These results are summarized in Table 3.2 in the form of the statistical 95% confidence intervals across measurements from each pulse of all six microthrusters. Ultimately, the triple probe indicates that the electron temperature of the microthruster plume is typically between 1 and 2 eV, which is roughly equal to that seen in some electrothermal PTFE PPT's [5, 25]. The electron density measured is between 10^{11} to 10^{14} cm^{-3}, which is quite

low relative to PTFE PPT's [5, 25], and more akin to that of MPD thruster plumes. Additionally, the variability of the electron temperature peak measurement is different across thrusters, but overall is about 40%. The density measured varies greatly from thruster to thruster, and thus a simple range estimate is reported here, along with the measurements from each microthruster.

Table 3.2: Confidence intervals for peak electron temperature and density from LTP measurements.

Serial No.	Pulses	95% CI Peak T_e (eV)	95% CI Peak n_e (cm-3)
OD02A10	150	2.1 ± 0.2	2.3E+12 ± 1.6E+11
RR51A03	150	2.0 ± 0.5	2.3E+11 ± 1.6E+10
RR51A06	150	1.7 ± 0.1	3.4E+12 ± 1.3E+12
RR51A10	150	1.6 ± 0.1	2.4E+14 ± 1.7E+13
RR52A10	149	1.2 ± 0.4	2.8E+11 ± 2.0E+10
Overall:		1.7 ± 0.7	$10^{11} – 10^{14}$

3.5. RGA RESULTS

Residual gas analysis of the plume estimates the gas species present in the exhaust mixture of the microthruster. Incoming particles are ionized and exposed to a quadrupole mass spectrometer that filters the particles by mass. Typically, an RGA system is operated in a "mass sweep" mode, where the partial pressure of all species in the chosen range are detected and displayed. However, this process is too slow to capture the plume species for the ESP microthruster. Thus, a "trend" mode was employed whereby specific mass values (8 in this case) are continuously recorded. We observed eight different mass values corresponding to the most probable plume constituents based on the ESP composition (HAN, PVA, AN), combustion products (N_2, H_2, CO_2, H_2O, C_2) as well as decomposition intermediates such as nitric acid (HNO_3), nitrous acid (HONO), hydroxylamine (NH_2OH) and other nitrogen oxides. The RGA measures the temporal evolution of the partial pressure for each of these mass values. Data are acquired for each of 40 pulses of a single microthruster, 20 pulses in the early lifetime (pulses 1-20), and 20 pulses in the later lifetime (pulses 50-70). For each mass the average change in the

partial pressure over all 40 pulses is calculated. These values are reported in Table 3.3, along with the possible plume species that could contribute to the measured increase in partial pressure. A scan for partial pressure of nitric acid (HNO_3, MW=63 g/mol) did not reveal a signal from the RGA, though a number of other intermediates and exhaust species were detected.

Table 3.3: Average increases in partial pressure of each species in RGA results.

MW (g/mol)	Species	Average ΔP (Torr)
2	H_2	4.84E-08
12	C_2	1.85E-06
18	H_2O	2.70E-06
28	N_2, NO	9.83E-07
32	O_2, NH_2OH	4.74E-07
44	CO_2, PVA, NO_2, HONO	2.11E-07
80	AN	1.48E-06
96	HAN	1.74E-06

4. ANALYSIS AND DISCUSSION

Experimental results are used to determine the total plume charge and ionization fraction. Further results are used to determine an effective exhaust velocity of the plume. Direct measurements of effective exhaust velocity agree well with indirect calculations from mass bit and impulse bit measurements. A thermal equilibrium and adiabatic expansion analysis suggest the exhaust is not in equilibrium, and that the electrons are at much higher temperature than the colder neutral species.

4.1. PLUME CHARGE

The measured current density shown in Figure 3.2 is integrated to determine the total charge collected at different radial and axial locations within the plume, according to equation (5). Figure 3.2 shows the results for variations in axial and radial locations, including 5, 7.5, 10, 15, 20, 30 and 40 cm downstream on-centerline and then 5, 10 and 15 cm radial locations for a 5cm downstream location.

$$Q_i = \int_{\mathbf{0}}^{t_d} I_p(t)\, dt \tag{5}$$

The peak collected charge is 4.3×10^{-5} C at the 5 cm location, and that value rapidly decreases with distance downstream to 50% of that peak at 10 cm, 20% at 20 cm and more than an order of magnitude lower at the 40 cm location, where the collected charge is calculated 4.0×10^{-6} C. Similarly, the results from the off-centerline testing in Figure 4.1b shows a peak value of 4.2×10^{-5} C at the centerline location that decreases by 75% at 5 cm in the radial direction, more than an order of magnitude at 10 cm (1.6×10^{-6} C), and becomes negligible (< 0.1 μC) relative to the peak at 15 cm or more off-centerline. Results are quite consistent across the samples taken of 100-150 pulses on three separate microthrusters, and the 95% confidence intervals are shown for these calculations. These results indicate that the majority of the charged particles present in the thruster plume are contained in the radial region from -10 to 10 cm. Since these measurements were taken at a distance of 5 cm downstream of the thruster, this indicates

that the plume divergence half-angle is 60° or greater. These results are used to determine the number of charged particles present in the plume relative to the neutrals.

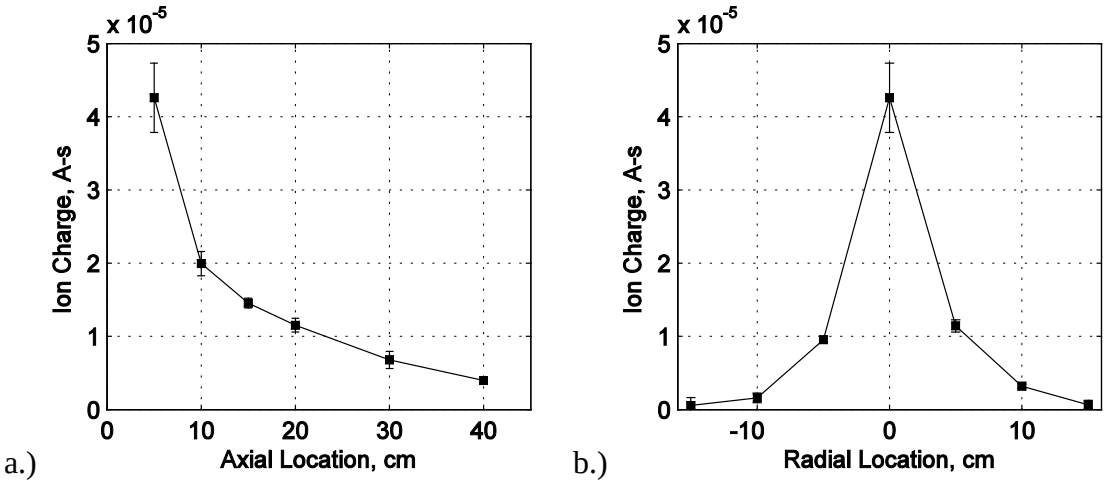

Figure 4.1: Integrated Faraday Probe results indicating total ion charge collected in Coulombs for the a.) centerline locations and b.) off-centerline locations.

4.2. PLUME COMPOSITION

The composition of the ESP is well understood (Table 2.1), as well as the product species of theoretical *full* combustion/decomposition of the propellant [3]. However, due to the very short pulse and resident times in the operation of the microthruster, it is unlikely that full combustion of the propellant is achieved. To characterize the exhaust species of the ESP, the RGA data from Table 3.3 was used. For a given pulse, the increase in partial pressure for each species is compared to the increase in total pressure (i.e. the sum of all the increases in partial pressures) to determine the fraction of species present (or rather, detected) in that pulse. Extending this method to the 40 pulse sample of the thruster and averaging the results gives an average makeup by percent, based on the increase in partial pressure. Combining this information with the molecular weight of each species provides an accurate estimate of the *actual* gas species present in the exhaust plume of the thruster. Figure 4.2 below presents these estimates compared with the product species predicted from full combustion of the ESP. The data of Figure 4.2 are a time-averaged molecular weight of the exhaust gas mixture. Using this plume

composition, the exhaust gas mixture molecular weight is calculated to be 43 g/mol. This is the molecular weight used in equation (2) for triple Langmuir probe calculations.

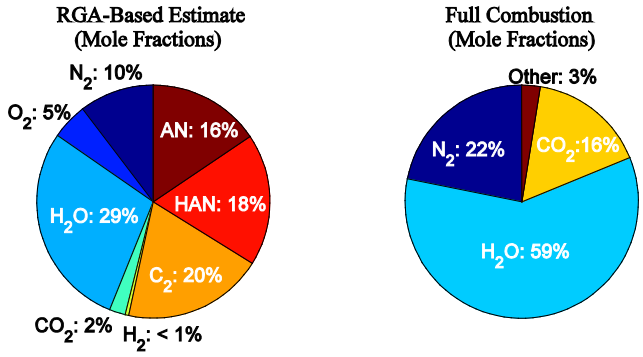

Figure 4.2: Plume exhaust gas species comparison.

The results from the residual gas analysis confirm the hypothesis that the propellant does not have a sufficient residence time to undergo full decomposition. In fact, raw propellant material (HAN, AN, perhaps PVA) are detected in the exhaust gas, in addition to combustion intermediates and products. The presence of materials from each of these stages suggests that the plume is in a "frozen flow" state, which could contribute to propellant use inefficiency in the current configuration. Detection of raw propellant material also suggests that the ESP material may suffer from particulate generation during a pulse (or following one). Particulate emission at low velocity has been observed in PTFE PPTs, and has been identified as one of the dominant sources of propellant utilization inefficiency [19].

4.3. PLUME IONIZATION FRACTION

Plume ionization fraction is estimated using the total charge calculations and plume composition calculations. The ionization fraction is calculated by dividing the total number of emitted charged particles by the total number of emitted particles during a single pulse. Total collected charge was calculated and presented for various locations in Figure 3.2. We assume the plume to be axially symmetric, in which case the data of Figure 3.2b can be integrated over a hemisphere of the plume to yield the total charge emitted from the thruster. We assume all emitted charged particles are singly ionized

since the measured electron temperature is on the order of 1-2 eV, and the ionization potential for plume species are on the order of 13-15 eV, it is unlikely that a significant multiply-charged ion population exists. With these assumptions the total number of charge carriers is estimated to be on the order of 10^{14} emitted charged particles per pulse. Number of total emitted particles is determined using the measured average mass bit (Table 3.1), the measured plume composition (Figure 4.2), and the known molecular weight of each plume species. On average this results in $3x10^{16}$ total emitted particles per pulse. The results indicate an ionization fraction of 0.31% ± 0.03%. The ionization fraction is much lower than is typically measured in the plume of a PTFE PPT, which is typically 10 – 20% [5]. This lower ionization fraction is likely due to the lower electron temperature (1-2 eV vs. 4-5 eV) and voltage of electric discharge (300 V vs. 1-2 kV), resulting in less ionization of the exhaust gas.

4.4. EFFECTIVE EXHAUST VELOCITY

Effective exhaust velocity was determined two different ways showing good agreement and lending confidence to the results. It was calculated from time-of-flight measurements and it was calculated from measured mass bit and impulse bit results. The triple probe results were used to calculate the time-of-flight of the plume exhaust from the thruster exit to the probe. The distance of travel is known (5 cm), and we define the time-of-flight to be the time between when the discharge current measurement becomes positive (time zero) and the time of peak current measured by the triple probe (~20 to ~60 μs). Due to an inadequate temporal resolution of the data acquisition system the accuracy of this time of flight is ±4 μs, limiting the determination of the time-of-flight to an ~10% uncertainty. Additionally, velocity was calculated from impulse bit and mass bit results. The measured impulse bit (Figure 3.1) is divided by the measured average mass bit (Table 3.1) for the respective thruster. Results of these calculations are shown in Figure 4.3. Time-of-flight results indicate an average exhaust velocity over all pulses of about 1500 m/s, while the impulse bit and mass bit calculations suggest a 10% higher exhaust velocity of about 1650 m/s. The calculations shown in Figure 4.3a have a combined standard deviation of about 576 m/s, which is dominated by microthruster RR43A08. The high shot-to-shot variation of the time-of-flight calculated velocity is likely due to the intrinsic shot-to-shot variations of the microthrusters, as seen in the previous results.

It may also be affected by the large observed plume divergence half angle, leading to a less uniform axial velocity. The impulse bit and mass bit velocity calculations do not exhibit as much shot-to-shot variation because the average mass bit is used in the calculation, the actual mass bit for a given shot is unknown. The calculated velocities of Figure 4.3 are on the order of typical mass-averaged PPT plume velocities (3-5 km/s), but much slower than typical ion/charged particle velocities observed in PTFE PPT's, which are 10-50 km/s [5, 29, 30].

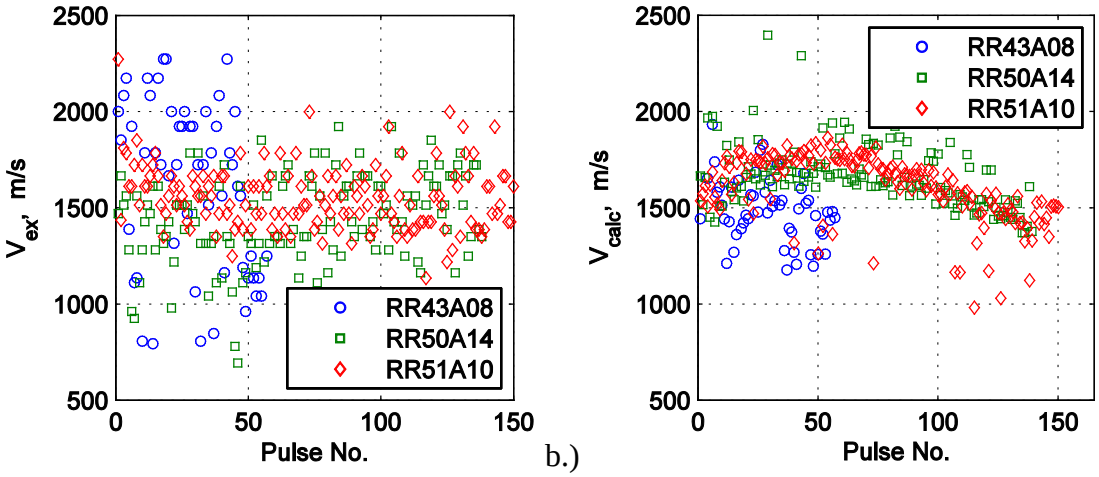

a.) b.)

Figure 4.3: Exhaust velocity calculated using (a) time-of-flight and (b) measured impulse bit and mass bit.

4.5. NON-THERMAL EQUILIBRIUM EXHAUST

Thermal equilibrium and adiabatic expansion calculations are presented and results suggest a non-thermal equilibrium exhaust gas, possibly a two temperature exhaust. Ionization at thermal equilibrium is governed by the Saha Equation, equation (6). The microthruster exhaust is composed of multiple species with different ionization potential, θ_i. These exhaust species have ionization potential ranging from 13-15 eV, and we assume the ionization potential is 13 eV for this analysis. The ionization fraction does not vary substantially within this range. We also assume the internal partition functions do not change between the neutral and ionized species. Using the Saha equation the ionization fraction as a function of temperature and pressure is calculated and shown in Figure 4.4.

The microthruster exhaust gas is not in thermal equilibrium. Experiments measured a plume electron temperature of 1-2 eV (10,000-20,000 K). If the gas were in thermal equilibrium at 1-2 eV, then an ionization fraction of 0.01 – 0.2 (1-20%) is expected. Measurements indicate an ionization fraction an order of magnitude lower at 0.003 (0.3%). The measured level of ionization of 0.003 suggests a thermal equilibrium temperature of 5500 – 8000 K; however, additional results suggest the actual exhaust gas temperature is much lower.

$$\frac{\phi^2}{1-\phi^2} = \frac{1}{p}\left(\frac{2m_e\pi}{h^2}\right)^{3/2}(kT)^{5/2}\frac{2\prod_{\text{int}} Q_{\text{int}}^{Z^+}}{\prod_{\text{int}} Q_{\text{int}}^{Z}}\exp\left(-\frac{\theta_i}{T}\right) \tag{6}$$

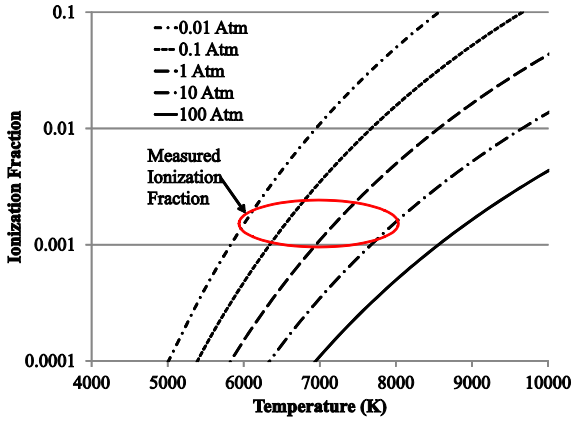

Figure 4.4: Equilibrium ionization as a function of temperature and pressure.

Conservation of energy requires the exhaust velocity of the gas to be equal to the difference in the total and static enthalpy according to equation (7), assuming there is no contribution from chemical reactions in the propellant. Given the indication of frozen flow in residual gas analysis results, we believe this is a valid assumption. The molecular weight of the exhaust mixture is assumed to be 43 g/mol based on the RGA measurements. Further we assume the exhaust temperature of the gas is much lower than the internal chamber temperature ($T_e \ll T_c$). The predicted exhaust velocity as a function of specific heat ratio and chamber temperature is given in Figure 4.5. Based on the calculated exhaust velocity (from both time-of-flight and impulse bit/mass bit) the temperature of the gas inside the thruster is 1500-2500 K.

The results suggest a non-thermal equilibrium possibly two temperature plume exhaust. During the microthruster discharge the neutral and ion species are heated to a temperature of 1500-2500 K. Charged particle production (ionization) is not driven by thermal electron impact processes because the temperature is too low (lower than the 5500-8000 K required to achieve 0.3% ionization fraction). Instead the ionizing energy of the electrons is obtained directly through the voltage and electric field of the electric discharge (300 V). The result is an electron population with a temperature of 1-2 eV. While the electrons are much hotter than the neutral and ion species, the expansion and acceleration of the mixture is governed by the heavy species, and thus the entire expelled gas has an effective exhaust velocity of 1500-2000 m/s.

$$u_e = \sqrt{2\frac{\gamma\Re}{(\gamma-1)MW}(T_c - T_e)} \approx \sqrt{2\frac{\gamma\Re}{(\gamma-1)MW}T_c} \tag{7}$$

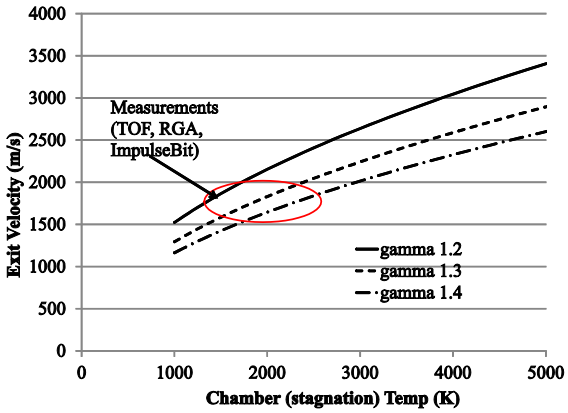

Figure 4.5: Exit velocity calculated assuming adiabatic expansion.

5. CONCLUSION

This experimental characterization of the plasma plume of a solid electric propellant microthruster was conducted with the goal of understanding the physics of the novel electric solid propellant, HIPEP, and the performance of the microthruster as a pulsed plasma thruster device. The diagnostics employed included a nude Faraday probe, a triple Langmuir probe and a residual gas analyzer. Centerline ion current density measurements were made at 5, 7.5, 10, 15, 20, 30 and 40 cm downstream location, and 5, 10 and 15 cm off-centerline in two directions. The peak ion current density measured was about 273 mA/cm^2, observed at a location on the centerline of the thruster at 5 cm downstream. Electron temperature and density measurements were also made using a triple Langmuir probe on centerline at 5 cm downstream. Overall, measurements of peak electron temperature were about 1.7 eV and peak electron density between 10^{11} and 10^{14} cm^{-3}. Ablation mass characterization yields an average mass bit of about 215 μg. Extending the plasma measurements to this value yields an ionization fraction of 0.3% of the ablation mass. Further, time-of-flight measurements, and impulse bit and mass bit measurements, indicate a plume exhaust velocity of about 1500-1650 m/s. Analytical calculations suggest a non-equilibrium plume gas composed of hot electrons (1-2 eV) and colder neutral and ion species (1500-2500 K).

Experimental results indicate significant variations from pulse to pulse and from thruster to thruster. Impulse bit can vary by as much as 40% over the thruster lifetime, and 60% from thruster to thruster. Plume temperature can vary by over 50% from thruster to thruster, and typically decreases by a factor of 2 or more in early thruster lifetime. Electron density does not vary considerably over pulse lifetime, but can vary by up to 3 orders of magnitude from thruster to thruster. The exact causes of this variation are not yet known, though two main candidates have been identified: inconsistencies in the solgel propellant filling process and variations in the chemical makeup of large batches of the propellant. Inconsistencies in the solgel propellant filling process (viscous liquid injected by hand into microthruster) are perhaps the most likely as it is a variable process. Human inconsistency could lead to slight variations in the cured propellant between thrusters. Further, the cured propellant may not be entirely uniform in each

microthruster. Structural variations in the propellant such as voids, density gradients or grain changes may exist in a given microthruster, but are unable to be visually observed. This could lead to the observed pulse-to-pulse and thruster-to-thruster variation. On a larger scale, variations in the chemical makeup may exist in the large batches of uncured propellant that is then used to assemble many microthrusters. These variations are expected to be minimal between batches as the materials and processes used are not substantially different.

Despite the observed fluctuations of plume properties, results suggest the thruster plume is a weakly ionized gas consisting of high temperature electrons in a low relative temperature ions and neutrals. The acceleration mechanism is thus dominated by electrothermal energy, a property typical of some “electrothermal” PPT’s. Thermal inefficiency is evident in the low temperature and density plume relative to PTFE PPT plumes despite a stored energy (40 J) in the upper regime of PPT operation. This suggests that much of the thermal energy generated by the discharge is deposited into the electrodes or other parts of the thruster (i.e. not the propellant). Further, the propellant may suffer from inefficient propellant utilization mechanisms like those observed in PTFE, as well as frozen flow losses, though additional investigation is required. Ultimately, the HIPEP material behaves similar to PTFE, but the plume has a lower electron temperature, electron density and ionization fraction, and a larger ablation mass bit in this configuration. However, further study of the propellant is desired, particularly identifying key differences in the physical mechanisms of the propellant ablation [31] in comparison to PTFE.

REFERENCES

[1] Sawka, W. N., "Pulse Performance and Power Requirements for Electrically Controlled Solid Propellant," *54th JANNAF Propulsion Meeting*, JANNAF, Denver, CO, 2007.

[2] Sawka, W. N., Katzakian, A., and Grix, C., "Solid State Digital Cluster Thrusters for Small Satellites, Using High Performance Electrically Controlled Extinguishable Solid Propellants," *AIAA/USU Conference on Small Satellites*, AIAA, Logan, UT, 2005.

[3] Sawka, W. N., and McPherson, M., "Electrical Solid Propellants: A Safe, Micro to Macro Propulsion Technology," *49th AIAA/ASME/SAE/ASEE Joint Propulsion Conference*, AIAA, San Jose, CA, 2013. doi: 10.2514/6.2013-4168

[4] Sawka, W. N., U.S. Patent for a "Controllable Digital Solid State Cluster Thrusters for Rocket Propulsion and Gas Generation," No. 7958823 B2 and 8464640; June 14, 2011 and June 18, 2013.

[5] Burton, R. L., and Turchi, P. J., "Pulsed Plasma Thruster," *Journal of Propulsion and Power*, Vol. 14, No. 5, 1998, pp. 716-735. doi: 10.2514/2.5334

[6] Guman, W. J., and Peko, P. E., "Solid-Propellant Pulsed Plasma Microthruster Studies," *Journal of Spacecraft and Rockets,* Vol. 5, No. 6, 1968, pp. 732-733. doi: 10.2514/3.29340

[7] Guman, W. J., and Nathanson, D. M., "Pulsed Plasma Microthruster Propulsion System for Synchronous Orbit Satellite," *Journal of Spacecraft and Rockets*, Vol. 7, No. 4, 1970, pp. 409-415. doi: 10.2514/3.29955

[8] LaRocca, A. V., "Pulsed Plasma Thruster System for Attitude and Station Control of Spacecraft," *First Western Space Congress*, 1970, pp. 688-702.

[9] Vondra, R. J., and Thomassen, K. I., "Flight Qualified Pulsed Electric Thruster for Satellite Control," *Journal of Spacecraft and Rockets*, Vol. 11, No. 9, 1974, pp. 613-617. doi: 10.2514/3.62141

[10] Gatsonis, N. A., Lu, Y., Blandino, J., Demetriou, M. A., and Paschalidis, N., "Micropulsed Plasma Thrusters for Attitude Control of a Low-Earth-Orbiting Cubesat," *Journal of Spacecraft and Rockets*, Vol. 53, No. 1, 2016, pp. 57-73. doi: 10.2514/1.A33345

[11] Rayburn, C. D., Campbell, M. E., and Mattick, A. T., "Pulsed Plasma Thruster System for Microsatellites," *Journal of Spacecraft and Rockets,* Vol. 42, No. 1, 2005, pp. 161-170. doi: 10.2514/1.15422

[12] Rudolph, L. K., Pless, L. C., and Harstad, K. G., "Pulsed Plasma Thruster Backflow Characteristics," *Journal of Spacecraft and Rockets,* Vol. 17, No. 5, 1980, pp. 447-452. doi: 10.2514/3.57763

[13] Janson, S., "The on-Orbit Role of Electric Propulsion," *29th Joint Propulsion Conference and Exhibit,* AIAA, Monterey, CA, 1993. doi: 10.2514/6.1993-2220

[14] Vondra, R. J., and Thomassen, K. I., "Performance Improvements in Solid Fuel Microthrusters," *Journal of Spacecraft and Rockets,* Vol. 9, No. 10, 1972, pp. 738-742. doi: 10.2514/3.61794

[15] Solbes, A., Thomassen, K., and Vondra, R. J., "Analysis of Solid Teflon Pulsed Plasma Thruster," *Journal of Spacecraft and Rockets,* Vol. 7, No. 12, 1970, pp. 1402-1406. doi: 10.2514/3.30181

[16] Boyd, I. D., Keidar, M., and McKeon, W., "Modeling of a Pulsed Plasma Thruster from Plasma Generation to Plume Far Field," *Journal of Spacecraft and Rockets,* Vol. 37, No. 3, 2000, pp. 399-407. doi: 10.2514/2.3574

[17] Jahn, R. G., *Physics of Electric Propulsion*, New York: McGraw-Hill, 1968.

[18] Liebing, L., and Seidel, F., "Low Current Pulsed Ablation Plasma Thruster," *Journal of Spacecraft and Rockets*, Vol. 11, No. 9, 1974, pp. 609-610. doi: 10.2514/3.62139

[19] Spanjers, G. G., Lotspeich, J. S., McFall, K. A., and Spores, R. A., "Propellant Losses Because of Particulate Emission in a Pulsed Plasma Thruster," *Journal of Propulsion and Power,* Vol. 14, No. 4, 1998, pp. 554-559. doi: 10.2514/2.5313

[20] Sigma-Aldrich, "Ionic Liquids for Electrochemical Applications," *Aldrich ChemFiles,* Vol. 5, No. 6, 2005.

[21] Lau, M., Manna, S., Herdrich, G., Schönherr, T., and Komurasaki, K., "Investigation of the Plasma Current Density of a Pulsed Plasma Thruster," *Journal of Propulsion and Power,* Vol. 30, No. 6, 2014, pp. 1459-1470. doi: 10.2514/1.B35131

[22] Walker, M. L. R., Victor, A. L., Hofer, R. R., and Gallimore, A. D., "Effect of Backpressure on Ion Current Density Measurements in Hall Thruster Plumes," *Journal of Propulsion and Power,* Vol. 21, No. 3, 2005, pp. 408-415. doi: 10.2514/1.7713

[23] Chen, S.-L., "Studies of the Effect on Ion Current on Instantaneous Triple-Probe Measurements," *Journal of Applied Physics,* Vol. 42, No. 1, 1971, pp. 406-412. doi: 10.1063/1.1659611

[24] Chen, S.-L., and Sekiguchi, T., "Instantaneous Direct-Display System of Plasma Parameters by Means of Triple-Probe," *Journal of Applied Physics*, Vol. 36, No. 8, 1965, pp. 2363-2375. doi: 10.1063/1.1714492

[25] Eckman, R., Byrne, L., Gatsonis, N. A., and Pencil, E. J., "Triple Langmuir Probe Measurements in the Plume of a Pulsed Plasma Thruster," *Journal of Propulsion and Power,* Vol. 17, No. 4, 2001, pp. 762-771. doi: 10.2514/2.5831

[26] Gatsonis, N. A., Eckman, R., Yin, X., Pencil, E. J., and Myers, R. M., "Experimental Investigations and Numerical Modeling of Pulsed Plasma Thruster Plumes," *Journal of Spacecraft and Rockets*, Vol. 38, No. 3, 2001, pp. 454-464. doi: 10.2514/2.3704

[27] Eckman, R., "Pulsed Plasma Thruster Plume Diagnostics," *36th AIAA Aerospace Sciences Meeting and Exhibit*, AIAA, Reno, NV, 1998. doi: 10.2514/6.1998-4

[28] Tilley, D. L., Kelly, A. J., and Jahn, R. G., "The Application of the Triple Probe Method to Mpd Thruster Plumes," *21st International Electric Propulsion Conference*, AIAA, Orlando, FL, 1990. doi: 10.2514/6.1990-2667

[29] Schönherr, T., Komurasaki, K., and Herdrich, G., "Propellant Utilization Efficiency in a Pulsed Plasma Thruster," *Journal of Propulsion and Power,* Vol. 29, No. 6, 2013, pp. 1478-1487. doi: 10.2514/1.B34789

[30] Thomassen, K., and Vondra, R. J., "Exhaust Velocity Studies of a Solid Teflon Pulsed Plasma Thruster," *9th Aerospace Sciences Meeting*, AIAA, New York, NY, 1971. doi: 10.2514/6.1971-194

[31] Keidar, M., Boyd, I. D., and Beilis, I. I., "Model of an Electrothermal Pulsed Plasma Thruster," *Journal of Propulsion and Power,* Vol. 19, No. 3, 2003, pp. 424-430. doi: 10.2514/2.6125

II. OBSERVATION OF LATE-TIME ABLATION IN ELECTRIC SOLID PROPELLANT PULSED MICROTHRUSTERS

Matthew S. Glascock and Joshua L. Rovey,
Missouri University of Science and Technology, Rolla, Missouri, 65409
and
Shae Williams and Jason Thrasher,
Digital Solid State Propulsion, Reno, Nevada, 89511

ABSTRACT

Electric solid propellants are an interesting potential option for propulsion because they are ignited by an applied electric current. The electric nature of these materials leads to the capability for use in pulsed electric propulsion devices. In this work, the ablation process of an electric solid propellant during pulsed microthruster operation is investigated using a triple Langmuir probe, thrust stand and high speed video camera. Results include quantitative time-of-flight, ablation mass per pulse and impulse-per-pulse measurements. Additionally, qualitative images from the high speed video are temporally correlated to these measurements. Analyses indicate 45±11% of the ablated mass per pulse is expelled at negligible speeds relative to the effective plume exhaust velocity (1500 m/s). Further, this occurs on a time scale that is three times longer than the 0.5 ms primary discharge. This late-time ablation has been identified in other pulsed microthrusters with traditional Teflon propellant, and the results presented here indicate that electric solid propellant exhibits similar behavior.

1. INTRODUCTION

Electric solid propellants (ESP's) are an emerging topic of research with major implications in the field of propulsion from the micro to macro scale [1,2]. These propellants offer new capabilities for controlling solid chemical rocket motors previously unheard of for typical energetic materials. When electric power at sufficient current and voltage levels is applied to an ESP, the solid propellant ignites and continues to exothermically decompose until that power is removed. This process can be repeated until the solid propellant is entirely consumed. Further, the burn rate of the propellant can be throttled by altering the electrical power applied. This method of operation is not possible with traditional solid rocket propellants and energetics, and greatly expands the potential applications for solid rocket motors that are fit with an ESP. Additionally, ESPs are insensitive to accidental ignition by spark, impact or even open flame. This is a huge advantage over most energetics in safety considerations and ease of use.

The development of ESPs began in the mid-late 90's with the investigation of a "green" automobile air bag inflator propellant (ABIP). This ammonium nitrate based material quickly garnered attention from the U.S. Air Force for other applications, including a patented [3] formulation for rocket propulsion application. Soon after, the first controlled extinguishable solid propellants were developed, the first of which was referred to as "ASPEN." This development process began adding ingredients to the ammonium nitrate based propellant to lower the melting point and increase the electrical conductivity during chemical combustion. Performance metrics of the ASPEN propellant were comparable to typical marks for solid rocket motors, but experienced major problems with initial ignition. Addressing these problems led to the development of a more advanced formula to achieve higher specific impulse and conductivity of the propellant. This higher performance electric propellant (HIPEP) is a hydroxyl ammonium nitrate (HAN) based energetic material. In this formulation, the ionic liquid oxidizer HAN exhibits a pyroelectric behavior; the application of electric power to this material incites the creation of nitric acid, triggering ignition of the formulation. This behavior has been previously observed in organic materials, but none of which are known to be energetic.

Electric solid propellants have also been tested for application in electric propulsion. All of the aforementioned ESP's have been tested as alternative fuel/propellant for the ablation fed pulsed plasma thruster and have shown performance marks comparable to that of the traditional propellant [2]. The Pulsed Plasma Thruster [4] (PPT) is a type of in-space electric propulsion system first flown in November of 1964 aboard the Soviet spacecraft Zond 2, marking the first application of electric propulsion on a spacecraft. Modern PPTs are primarily used for stationkeeping needs, attitude control, and other secondary propulsion system duties [5-7]. These thrusters have received considerable attention in the propulsion community due to the relative simplicity of the supporting technology and their ability to reliably generate small impulse bits.

Operation of the ablation-fed PPT begins with a high-current discharge between electrodes across the exposed surface of a solid propellant, usually Teflon® (PTFE). Typically, PPTs fall within two distinct classes of electric propulsion: electrothermal or electromagnetic [8]. The key difference lies in the acceleration mechanisms observed in PPT operation. LES 8/9 exhibits a typical behavior in that a portion of the plume is ionized by the main discharge (~10% in this case) and accelerated by the electromagnetic force arising from the $j \times B$ current front that propagates along with the ablated mass [8]. These high-energy, high-velocity particles contribute 15% (or more) of the kinetic energy of the exhaust gas despite the low mass relative to the rest of the plume, which remains neutral. On the other hand, the PPT-3/PPT-4 design is less common in that the acceleration of the ablated mass is dominated by electrothermal effects [9]. The temperature arising from the arc discharge is sufficiently high to provide enough energy to the particles to provide exhaust velocities comparable to or even exceeding that of chemical thrusters. These temperatures are typically limited by radiation and other dissipative processes to a few eV, but the high temperature neutrals provide nearly the entirety of the kinetic energy in the exhaust. Additionally, both thrusters (and most PPTs in general) have shown evidence of lost mass after the completion of the discharge pulse in the form of low relative velocity neutrals and even macroparticles [10]. This "late-time ablation" contributes little to nothing by way of performance. Further, this ablation is not readily measured, thus the mass fraction is not well characterized, but modeling efforts have estimated large fractions of the total ablated mass per pulse [11].

This paper focuses on the ablation of an electric solid propellant in PPT operation. Results from ablation mass, impulse-per-pulse and time-of-flight measurements are coupled with high speed imagery to show that the electric solid propellant exhibits late-time ablation. The experimental apparatus is described in Section 2, and the Results and Analysis are given in Section 3 and 4, respectively. Conclusions from the work are described in Section 5.

2. EXPERIMENTAL APPARATUS

The PPT microthrusters are described, along with the ESP and power processing unit. Then the facilities in which the microthrusters are operated are described, followed by the diagnostics used to characterize the thrusters.

2.1. MICROTHRUSTERS AND POWER PROCESSING UNIT

The microthrusters have a coaxial geometry as shown in Figure 2.1. The outer electrode is a 1/8" diameter aluminum tube and the concentric inner electrode is a 3/64" diameter molybdenum rod. The total length of the microthruster is about 1", with the propellant grain measuring roughly half of that length. The molybdenum inner electrode is also coated with polymer insulation (shellac) with a nominal thickness of 0.001". The ESP has a annular shape and fills the space between the inner and outer electrodes. By applying a relatively low voltage discharge from a capacitor bank (300 V) for a short duration pulse (about 0.5 ms) a small mass of the ESP is ablated and expelled from the thruster. In-house performance testing by the thruster manufacturer indicates that the impulse bit is around 500 μN-s per pulse, with a specific impulse on the order of 200 seconds. In general, the thrusters have an operation lifetime of between 250 and 300 pulses.

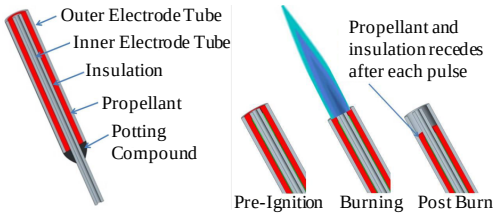

Figure 2.1: CAD Model illustrating composition and operation of the ESP microthruster.

The ESP is a hydroxyl ammonium nitrate (HAN)-based solution solid manufactured using benign processes and "green" ingredients, mixed in standard chemical glassware and cured conveniently at warm room temperatures (35°C/95°F). It has a chemical composition of HAN oxidizer (an inorganic ionic liquid) and polyvinyl alcohol (PVA) fuel binder, which make up 95% of the propellant, as shown in Table 2.1.

The ESP is initially a liquid and injected by syringe into the discharge gap of the microthruster. It is then cured to form a soft solid with the appearance and texture of a soft pencil eraser. It is safe to handle and classified under DOT as a 1.4S explosive, making this ESP much more convenient to transport and work with than conventional solid rocket propellants.

Table 2.1: Nominal composition of the High Performance Electric Propellant.

Chemical Name	Chemical Formula	Percentage by mass	Molecular Mass, g/mol
Hydroxyl Ammonium Nitrate (HAN)	$(NH_3OH)^+ NO_3^-$	75%	96
Polyvinyl Alcohol (PVA)	$CH_2CH(OH)$	20%	44
Ammonium Nitrate (AN)	NH_4NO_3	5%	80

There are some key differences between the ESP and traditional Teflon® (PTFE) PPT propellant. PTFE is a fluorocarbon solid, while the ESP is a soft-solid mixture with composition given in Table 2.1. In a typical PPT, the PTFE is an electrical insulator between the electrodes. The conductivity of the ESP in this work is comparable to "highly conductive" ionic liquids which have been selected as candidates for use in dye-sensitized solar cells [12]. With the ESP propellant the pulsed electric current can be conducted through the ESP, potentially initiating thermoelectric decomposition and creation of intermediates in the propellant. With PTFE an arc discharge is created near the surface of the solid PTFE, ablating the propellant via heat transfer. Additionally, in a conventional PPT, the propellant is fed into the thruster such that the arc discharge always occurs at the same physical location with respect to the thruster exit plane. With the ESP microthrusters the propellant face recedes from the exit plane over time as the propellant is burned away. It is currently unclear how these propellant differences affect the operation and performance of a PPT using the ESP as a propellant.

The power processing unit (PPU) used to operate the microthrusters is a custom in-house pulsed power supply. This PPU is primarily a bank of capacitors with a nominal

rating of 900 μF. This bank is charged to 300 V with a small input power (5 V at < 1A). Once charged, the stored energy (about 40 J) is then rapidly discharged directly into the thruster electrodes, an event which typically lasts about 500 μs. This mode of operation was chosen as it was shown to increase the total impulse delivered over the thruster lifetime. Additionally, the voltage level of 300 V was chosen to keep the impulse bit per pulse around 500 μN-s. This PPU is vacuum-compatible and is mounted a few inches from the thruster during testing; the PPU is then remotely controlled via serial communication.

2.2. VACUUM FACILITIES

2.2.1. Missouri S&T Aerospace Plasma Lab. The microthrusters were tested in the large (1.8 m dia., 3 m lg.) space and high altitude vacuum facility at the Aerospace Plasma Laboratory of Missouri S&T. This facility uses four 89 cm diameter oil vapor diffusion pumps backed by an Edwards EH 4200 roots-blower pump and a Tokunda KP-7500BG rotary-vane pump. Standard operation for this work was two oil vapor diffusion pumps active which gives the facility a nominal base pressure of 2×10^{-5} Torr. The interior of the facility is equipped with a two-axis translation table system with a minimum step size of 2.6 μm that is controllable remotely to allow for the measurements made at varying locations.

2.2.2. Digital Solid State Propulsion (DSSP) Vacuum Facility. Microthrusters were also tested in the large vacuum facility at DSSP. This facility uses a single Varian VHS-250 oil vapor diffusion pump and an Alcatel ADS501 model rotary-vane, roots-blower pump combination for roughing of the chamber. Standard operation for this work was with the oil vapor diffusion pump active, yielding a nominal base pressure of 5×10^{-4} Torr. The interior of the facility is equipped with an optical table for mounting of hardware and diagnostics.

2.3. DIAGNOSTICS

Characterization of the plasma plume created during a pulse is generally the first step of analyzing a PPT system, and the primary focus of this work. Plume velocity distribution, plasma density and temperature, and current density are very useful in analyzing performance of a PPT. Work on plasma plume characterization of the

microthruster has been conducted at Missouri S&T, who has partnered with DSSP to analyze the microthruster. A number of prevalent PPT plume diagnostics were prepared and used for the analysis of the microthruster. In this work, a Langmuir triple probe was used to determine plasma densities and temperatures as well as for time of flight measurements. Additionally, a mass balance and high speed camera were used to investigate the ablated mass per pulse.

2.3.1. Langmuir Triple Probe. The Langmuir Triple Probe (LTP) is used to measure electron density and electron temperature at various locations in the plume as a function of time. The triple probe is well suited to operation in pulsed environments, and is a common diagnostic for the pulsed plasma thruster [13,14]. Tungsten wire of 0.5 mm diameter was inserted into three bores of a quad-bore alumina tube, creating the three isolated probe tips with 5.0 mm of exposed length. The remaining bore is plugged with a ceramic adhesive. On the other end of the probe, the tungsten wires connect to individual standard RF cables inside a grounded enclosure to ensure the connections are well shielded.

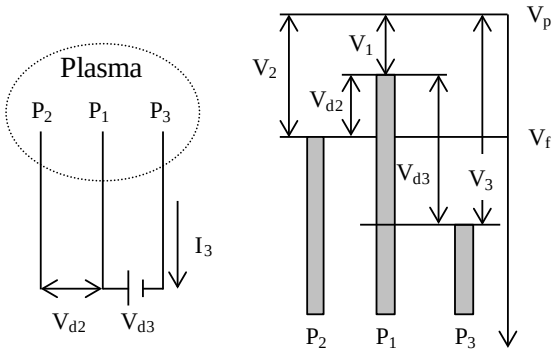

Figure 2.2: Electrical schematic and illustration of the triple Langmuir probe in voltage-mode.

In this work, the triple probe was operated in what is referred to as "voltage-mode," wherein (as in Figure 2.2) three identical probes are inserted into the plasma. All three probes are floating with respect to ground (V_f), and a bias voltage difference, V_{d3}, is applied externally to two of the probes via a battery. In this work, V_{d3} was selected as a nominal 27 V, supplied via three 9V batteries in series. During a pulse, the voltage

difference V_{d2} is measured via a differential voltage probe and the probe current, I_3, is measured via a current monitor. The high voltage differential probe was selected because these probes were found to be less susceptible to signal noise than digitally subtracting signals on an oscilloscope, or using differential operational amplifiers. These measurements are displayed as a function of time during testing on a 4-channel Tektronix TDS2024B oscilloscope. Through the Langmuir Triple Probe theory from Chen and Sekiguchi [15] these measurements $V_{d2}(t)$ and $I_3(t)$ can be used to directly calculate the plasma electron temperature, $T_e(t)$, and the plasma density, $n_e(t)$. This process was conducted by the authors previously [16]. In the present work, the triple probe is used as a plume time-of-flight measurement device in order to evaluate the effective exhaust velocity of the microthruster. This is accomplished by examining the probe current, I_3. This signal is then temporally correlated to initiation of the thruster circuit discharge current, I_D, as measured by an IPC CM-1-MG current monitor to determine the plume time-of-flight.

2.3.2. Mass Balance. Additionally, the mass bit expelled per pulse is a quality of interest in the testing of the microthrusters. In order to estimate this, the mass of a microthruster is measured immediately prior to testing and again immediately following testing. The mass scale used was a Radwag AS310/C/2 which has a resolution of 0.1 mg and a quoted repeatability (standard deviation from 10 weighing cycles) of 0.1 mg. With careful tabulation of the number of pulses logged on a microthruster during testing, an estimate within 2% of the average mass expelled per pulse (the mass bit) value can be determined. This value will be important for the analysis of the thrust contribution of the plasma plume and analysis of the impulse-per-pulse.

2.3.3. Thrust Stand. The existing thrust stand previously built in-house for performance testing of the microthrusters was used in this work. This thrust stand is integrated into the DSSP vacuum facility, and was thus not available for testing in the S&T facility. The design is a pendulum using spring steel as a dampening method. The microthruster is mounted to a fixture suspended from an aluminum frame by two pieces of 2.5 cm wide spring steel to ensure minimal cross-axis movement. During each thruster discharge, the displacement of the fixture is measured by a laser displacement sensor with a resolution of 5 μm. This corresponds to a resolution in thrust measurement of about 1

mN for typical pendulum fixture mass. Estimated accuracy of the thrust stand is ±10% based on error analysis in the laser and chamber back pressure. In the current configuration, the thrust stand can measure the impulse-per-pulse (or impulse bit, I_{bit}) of the microthruster within a range of 0.025 mN-s to 5 mN-s.

2.3.4. High Speed Camera. The high speed camera for the visual ablation analysis of the microthruster is a Vision Research Inc. Phantom V7.3 model camera with a maximum framerate of 500,000 frames-per-second (fps). Due to restrictions on image resolution, however, the framerate used in this work was 125,000 fps. This correlates to an exposure time of 8 μs per image. The typical setting for the camera in this work was to capture 200 images during the thruster discharge (i.e. 1.6 ms of footage). Additionally, the camera was triggered digitally in sync with the microthruster via LabVIEW. Measurement of a digital output of the high-speed camera detailing when the camera is triggered allows for temporal correlation of the images to probe diagnostic data accurate to about one frame (±8 μs).

3. RESULTS

In this section, experimental results from the mass balance, triple Langmuir probe and thrust stand are presented. These results include the average mass bit of all thrusters tested in recent time and some impulse-per-pulse results for a few of these that were measured. Experimental results are used to determine an effective exhaust velocity of the plume and temporally correlated to high speed images.

3.1. ABLATION MASS

Table 3.1 details the results of the mass balance measurements made of the microthrusters tested, both during this work, as well as in previous work [16,17]. These thrusters are all at (or nearly at) the observed end-of-life. The average mass bit (m_{bit}) is calculated by subtracting the final from initial mass and dividing by the number of pulses. Overall, the average mass bit is 215.4 μg. Note that some of the microthrusters shown here were tested in the DSSP facility, while others were tested in the S&T facility. This result is on the order of typical values for a PTFE PPT, which is usually between 10 and 100 μg, though it is noticeably higher than typical values [4].

Table 3.1: Average ablation mass bit data for selected microthrusters.

Serial no.	Pulses	Initial Mass (mg)	Final Mass (mg)	Average Mass Bit (μg)
OD01A09	200	639	549	450.0
OD01A12	222	647	590	256.8
OD01A13	206	642	588	262.1
OD01A14	155	636	545	587.1
OD01A17	280	643	611	114.3
OD02A06	150	637	603	226.7
OD02A10	150	625	613	80.0
RR43A08	121	641	631	82.6
RR50A14	143	658	639	132.9
RR50A20	153	661	637	156.9
RR51A03	150	661	614	313.3
RR51A06	150	642	623	126.7
RR51A10	161	641	624	105.6
RR52A10	150	665	647	120.0
			Mean:	215.4

3.2. LANGMUIR TRIPLE PROBE

The Langmuir triple probe provides measurements of probe current (I_p) as a function of time for each pulse of a microthruster. Additionally, a current monitor measures the thruster circuit discharge current (I_D) for each pulse. Figure 3.1 shows typical traces of $I_p(t)$ and $I_D(t)$ measurements for a single pulse of thruster RR51A10. These data are used to calculate the time-of-flight of the thruster plume from the initiation of the discharge current (here, ~110 μs) and peak probe current (~150 μs).

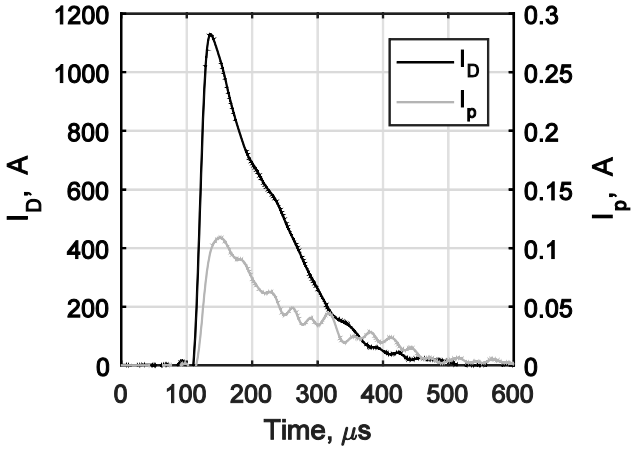

Figure 3.1: Typical thruster discharge and Langmuir triple probe current traces.

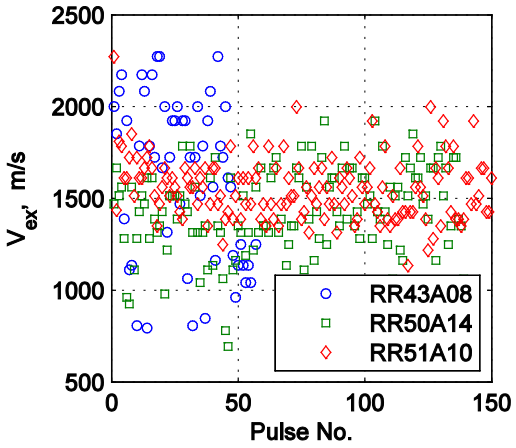

Figure 3.2: Effective exhaust velocity from Langmuir triple probe time-of-flight measurements.

Effective exhaust velocity (V_{ex}) was determined from these time-of-flight measurements, and the calculated data are shown in Figure 3.2. The three thrusters

shown were tested in the DSSP facility such that the impulse bit could be measured simultaneously with time-of-flight. The triple probe signal was used to calculate the time-of-flight of the plume exhaust from the thruster exit to the probe. The distance of travel is known (5 cm), and we define the time-of-flight to be the time between when the discharge current measurement becomes positive (i.e. time zero) and the time of peak current measured by the triple probe (~20 to ~60 μs). Time-of-flight results indicate an average exhaust velocity over all pulses of about 1500 m/s. Inadequate temporal resolution of the data acquisition system limits the accuracy of the determination of time-of-flight to ~10% uncertainty.

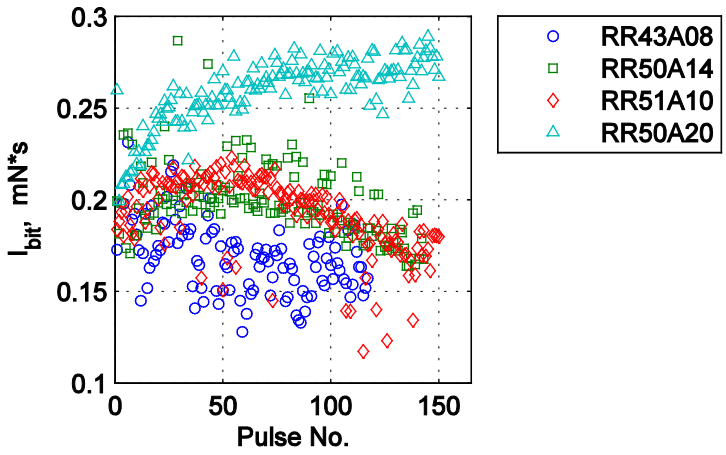

Figure 3.3: Measured impulse bit for four microthrusters.

3.3. IMPULSE BIT

Thrust testing was conducted at DSSP. A primary focus of this thrust testing was to determine the impulse bit per pulse (I_{bit}) of the microthrusters. Figure 3.3 shows these results over the pulse lifetime of four different microthrusters from various batches. The first three (RR43A08, RR50A14 and RR51A10) were tested in the DSSP vacuum facility equipped with the triple Langmuir probe diagnostic. The final thruster (RR50A20) tested previously by DSSP, was not interrogated with the Langmuir probe. From the data shown in Figure 3.3, the impulse bit is between 0.15-0.27 mN-s with an average value of 0.21 and 95% CI of ± 0.01 mN-s. The trends seen here are commonly observed for these microthrusters [2].

3.4. HIGH SPEED IMAGES

The Phantom high speed camera was used to capture images during the discharge of a small number of the thrusters tested. These images were then correlated with the measured discharge current of the thruster circuit. Figure 3.4 shows nine images taken from a single discharge with timestamps and corresponding time marks on the discharge circuit measurement. Note that the beginning of the discharge occurs at roughly 0.117 ms, as indicated by the rapid rise in discharge current and verified by the appearance of a visible glow at the thruster exit. Additionally, both the discharge current and the high speed images indicate a peak (peak current, peak visible intensity) at 0.133 ms, seeming to validate the correlation between the visible glow and the measured discharge current.

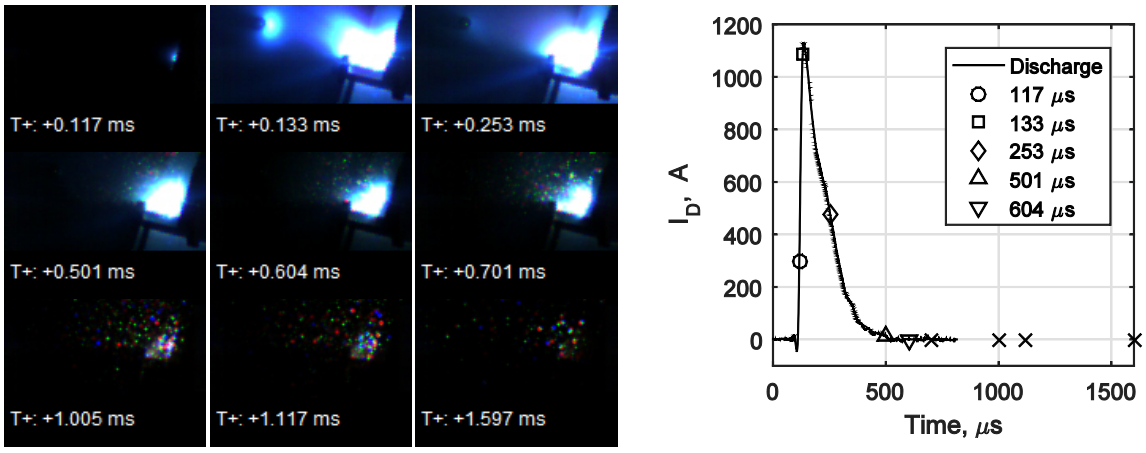

Figure 3.4: Selected images from high speed footage.

More interesting, however, is that the glow of the discharge and the apparent expulsion of particles are visible long after the discharge ends. The measured discharge current becomes negligible at the 0.501 ms timestamp, with a bright glow still visible. Further, even long after the discharge current is no longer measured, visible particles are observed, continuing through to the final image taken, at a timestamp of 1.597 ms. The time-scale for the total ablation is roughly three times that of the primary discharge. The ablation observed post-discharge is a previously studied phenomenon in PTFE PPTs, and is referred to as “late-time” ablation. Qualitatively, from the high speed imagery, it would seem that this ablated mass is a significant fraction of the total ablated mass per pulse, though there is no way to directly measure this fraction here.

4. ABLATION MASS ANALYSIS

The high speed imagery provides a qualitative indication of propellant ablation well after the main discharge has ended (late-time ablation). However, it is impossible to make a quantitative mass estimate for this ablated propellant without making restrictive and unfounded assumptions. Thus, it is desirable to apply the above numerical results to obtain some estimate of this late-time ablation mass. Using the simple equation (1) below, from the definition of impulse, the *calculated* ablated mass per pulse can be determined from the *measured* impulse bit and exhaust velocity. This calculation will then be compared to the directly measured ablation mass from this and previous work.

$$m_{bit} = \frac{I_{bit}}{V_{ex}} \tag{1}$$

Recall that m_{bit} is the ablation mass per pulse, I_{bit} the impulse per pulse and V_{ex} the effective exhaust velocity. Using the average values measured for these quantities (0.21 mN-s, 1500 m/s), an average calculated mass bit of 140 μg is obtained. This calculated mass bit is 65% of the measured average ablation mass bit (215 μg). This would indicate that the remaining 35% of the ablated propellant per pulse is ablating very slowly and not contributing to the measured impulse of each pulse. Looking at the specific cases of each microthruster, we find the average value to be 45±11% late-time ablation mass. Of course, this range is based on an average value, and some disagreement is to be expected for individual cases. For example, consider the three microthrusters for which both impulse-per-pulse and exhaust velocity measurement data are available: RR43A08, RR50A14 and RR51A10 (see Figure 3.2, Figure 3.3). From Table 3.1, we see the ablation mass measurements for these thrusters are 82.6, 132.9 and 105.6 μg, respectively. Comparing these values to the ablation mass calculated above indicates that all (or more) of the mass bit is necessary to produce the measured impulse bit at that velocity. This is nonsensical, and is likely due to a combination of measurement error and facility effects for these thrusters. More specifically, the DSSP test facility (where impulse bit can be measured) has a base pressure of more than twenty times that of the

facility used to test the other microthrusters. This raised back pressure will reduce the effective exhaust velocity from a time-of-flight measurement, falsely indicating that the entire ablation mass contributes to the measured impulse. Unfortunately, this data is only available for a select few thrusters. Nevertheless, we surmise that these are rough bounds for the actual late-time ablation mass fraction, and this sizeable fraction has been observed in PPTs previously.

The ablation process of PTFE has been investigated in detail by the PPT research community. Ablation modeling efforts have shown that the ablation is not an instantaneous process, but a gradual process correlated with the discharge current [11,18-20]. Experimental results have shown agreement with these conclusions [21]. Additionally, PPT experiments have identified residual heating, large particulate emission [10] and late-time material ablation [22] as causes of poor propellant efficiency in PPTs. Spanjers et. al [10] observed particulate emission in a PTFE PPT consuming 40±3% of the ablation mass and yet contributing less than 1% to thrust performance. Investigating post-pulse temperature effects, Antonsen et. al [22] found that late-time ablation accounted for 23±11% of the lost propellant. Clearly, these effects have a considerable negative impact on efficiency in PPTs. We have observed that these processes still occur when using an electric solid propellant in a PPT, with similar mass fractions.

5. CONCLUSION

Plume diagnostics were performed on a novel electric solid propellant microthruster. Twenty microthrusters were tested in two separate facilities. A Langmuir triple probe was used to measure the time-of-flight of the plume and an impulse-per-pulse of 0.21 mN-s was measured using a thrust stand. The average mass bit was found to be 215 μg from mass balance measurements. Analysis of the time-of-flight data yields an effective velocity of 1500 m/s. Additionally, high speed imagery of a microthruster during discharge shows evidence of late-time ablation of the electric solid propellant in the form of bright particles being expelled from the device long after the main discharge dissipates.

Numerical analysis of the measured impulse bit and exhaust velocity yields a calculated ablation mass that contributes to the impulse of 140 μg. This number differs from the measured ablation mass substantially and indicates that much of the ablation mass is expelled at low velocities and does not contribute meaningfully to the performance. The mass fraction of this late-time ablation is estimated to be 45±11%. Traditional pulsed plasma thrusters using PTFE for propellant experience a similar phenomenon with mass fractions on this order. Thus, we conclude that electric solid propellant exhibits the same behavior on a similar magnitude. Particulate emission and late-time ablation have been identified as causes of poor propellant efficiency in PPTs. Reduction of this late-time ablation during pulsed plasma thruster operation is an avenue of performance improvement for electric solid propellant.

REFERENCES

[1] Sawka, W. N., Katzakian, A., and Grix, C., "Solid State Digital Cluster Thrusters for Small Satellites, Using High Performance Electrically Controlled Extinguishable Solid Propellants," *AIAA/USU Conference on Small Satellites*, AIAA, Logan, UT, 2005.

[2] Sawka, W. N., and McPherson, M., "Electrical Solid Propellants: A Safe, Micro to Macro Propulsion Technology," *49th AIAA/ASME/SAE/ASEE Joint Propulsion Conference*, AIAA, San Jose, CA, 2013. doi: 10.2514/6.2013-4168

[3] Sawka, W. N., U.S. Patent for a "Controllable Digital Solid State Cluster Thrusters for Rocket Propulsion and Gas Generation," No. 7958823 B2 and 8464640; June 14, 2011 and June 18, 2013.

[4] Burton, R. L., and Turchi, P. J., "Pulsed Plasma Thruster," *Journal of Propulsion and Power*, Vol. 14, No. 5, 1998, pp. 716-735. doi: 10.2514/2.5334

[5] Gatsonis, N. A., Lu, Y., Blandino, J., Demetriou, M. A., and Paschalidis, N., "Micropulsed Plasma Thrusters for Attitude Control of a Low-Earth-Orbiting Cubesat," *Journal of Spacecraft and Rockets*, Vol. 53, No. 1, 2016, pp. 57-73. doi: 10.2514/1.A33345

[6] Guman, W. J., and Nathanson, D. M., "Pulsed Plasma Microthruster Propulsion System for Synchronous Orbit Satellite," *Journal of Spacecraft and Rockets*, Vol. 7, No. 4, 1970, pp. 409-415. doi: 10.2514/3.29955

[7] LaRocca, A. V., "Pulsed Plasma Thruster System for Attitude and Station Control of Spacecraft," *First Western Space Congress*, 1970, pp. 688-702.

[8] Jahn, R. G., *Physics of Electric Propulsion*, New York: McGraw-Hill, 1968.

[9] Boyd, I. D., Keidar, M., and McKeon, W., "Modeling of a Pulsed Plasma Thruster from Plasma Generation to Plume Far Field," *35th Joint Propulsion Conference and Exhibit*, AIAA, 1999. doi: 10.2514/6.1999-2300

[10] Spanjers, G. G., Lotspeich, J. S., McFall, K. A., and Spores, R. A., "Propellant Losses Because of Particulate Emission in a Pulsed Plasma Thruster," *Journal of Propulsion and Power*, Vol. 14, No. 4, 1998, pp. 554-559. doi: 10.2514/2.5313

[11] Mikellides, P., and Turchi, P., "Modeling of Late-Time Ablation in Teflon Pulsed Plasma Thrusters," *32nd Joint Propulsion Conference and Exhibit*, AIAA, Lake Buena Vista, FL, 1996. doi: 10.2514/6.1996-2733

[12] Sigma-Aldrich, "Ionic Liquids for Electrochemical Applications," *Aldrich ChemFiles*, Vol. 5, No. 6, 2005.

[13] Eckman, R., Byrne, L., Gatsonis, N. A., and Pencil, E. J., "Triple Langmuir Probe Measurements in the Plume of a Pulsed Plasma Thruster," *Journal of Propulsion and Power*, Vol. 17, No. 4, 2001, pp. 762-771. doi: 10.2514/2.5831

[14] Gatsonis, N. A., Eckman, R., Yin, X., Pencil, E. J., and Myers, R. M., "Experimental Investigations and Numerical Modeling of Pulsed Plasma Thruster Plumes," *Journal of Spacecraft and Rockets*, Vol. 38, No. 3, 2001, pp. 454-464. doi: 10.2514/2.3704

[15] Chen, S.-L., and Sekiguchi, T., "Instantaneous Direct-Display System of Plasma Parameters by Means of Triple-Probe," *Journal of Applied Physics*, Vol. 36, No. 8, 1965, pp. 2363-2375. doi: 10.1063/1.1714492

[16] Glascock, M. S., Rovey, J. L., Williams, S., and Thrasher, J., "Plume Characterization of Electric Solid Propellant Micro Pulsed Plasma Thrusters," *51st AIAA/SAE/ASEE Joint Propulsion Conference*, AIAA, Orlando, FL, 2015. doi: 10.2514/6.2015-4185

[17] Glascock, M. S., Rovey, J. L., Williams, S., and Thrasher, J., "Characterization of Electric Solid Propellant Pulsed Microthrusters," *Journal of Propulsion and Power*, (to be published).

[18] Gatsonis, N. A., Juric, D., Stechmann, D., and Byrne, L., "Numerical Analysis of Teflon Ablation in Pulsed Plasma Thrusters," *43rd AIAA/ASME/SAE/ASEE Joint Propulsion Conference & Exhibit*, AIAA, Cincinnati, OH, 2007. doi: 10.2514/6.2007-5227

[19] Keidar, M., Boyd, I. D., and Beilis, I. I., "Electrical Discharge in the Teflon Cavity of a Coaxial Pulsed Plasma Thruster," *IEEE Transactions on Plasma Science*, Vol. 28, No. 2, 2000, pp. 376-385.

[20] Schönherr, T., Zach, W. A., Komurasaki, K., Hörner, S., Arakawa, Y., and Herdrich, G., "Mechanical Probe and Modeling Efforts for Evaluation of Plasma Creation and Acceleration in Ppt," *33rd International Electric Propulsion Conference*, Washington, D.C., 2013.

[21] Scharlemann, C. A., and York, T., "Mass Flux Measurements in the Plume of a Pulsed Plasma Thruster," *42nd AIAA/ASME/SAE/ASEE Joint Propulsion Conference & Exhibit,* AIAA, Sacramento, CA, 2006. doi: 10.2514/6.2006-4856

[22] Antonsen, E. L., Burton, R. L., Reed, G. A., and Spanjers, G. G., "Effects of Postpulse Surface Temperature on Micropulsed Plasma Thruster Operation," *Journal of Propulsion and Power,* Vol. 21, No. 5, 2005, pp. 877-883. doi: 10.2514/1.13032

SECTION

2. CONCLUSIONS

The solid electric propellant pulsed microthruster has been characterized through experimental investigation. Primarily, this was conducted such that the behavior of the novel ESP used in this device configuration could be accurately described for use in future devices and applications. The key parameters of the plume created by this device like the electron temperature and density, ionization fraction, and effective velocity were examined. Further, the propellant mass ablated by the device per shot and the composition of this mass (i.e. the plume) were investigated. Measurements of the ablation mass and measured impulse per pulse were compared to those of exhaust velocity. High speed photography is also introduced to provide qualitative observations of this propellant ablation. These are properties typically measured in PTFE PPT research.

In this configuration, the ESP material behaves much like PTFE in a typical pulsed plasma thruster. Experimental results can vary greatly (up to 60% in some cases) from pulse to pulse and thruster to thruster. These variations are likely caused by inconsistencies in manufacture of the device. Despite these variations, general trends hold well enough to make the following conclusions. At 5 cm downstream of the device, the peak electron temperature is about 1.7 eV and the ion density is about 273 mA/cm^2, which suggests an ionization fraction of 0.3%. Correlating with this low percentage of charged particles is the measured electron density ($10^{11} – 10^{14}$ cm^{-3}), which is very low compared to PPTs. These results are very similar to PTFE PPTs, which are usually observed in the 1-10 eV range with ionization fractions of 1-10%. Additionally, the average ablation mass is about 215 μg. A significant portion (~45%) of this mass does not contribute to the measured impulse bit, likely being expelled at a very low velocity relative to the effective plume speed of about 1500 m/s. This behavior, known as late-time ablation, is an inefficient mechanism previously observed in a number PTFE PPTs, especially those dominated by electrothermal effects.

Despite these observed fluctuations, the overall results suggest the thruster creates a weakly ionized gas plume consisting of high temperature (1-2 eV) electrons in a low relative temperature (1500-2000 K) mixture of ions and neutrals. This plume is accelerated to its effective velocity by the thermal interaction in the thruster device. Due to radiation and other dissipative processes, the heavy particles can only receive a limited amount of energy via heat transfer, thus limiting this velocity to a few km/s. In this configuration, there is likely no electromagnetic acceleration of the bulk of the plume, due to negligible induced magnetic field during discharge. These effects are often observed in electrothermal PPTs using PTFE as propellant, thus it is concluded that the pulsed microthrusters in this work operate similar to these devices.

VITA

Matthew Scott Glascock was born in 1992 in Emporia, Kansas shortly before relocating to West Plains, Missouri where he spent the rest of his childhood. From a young age, he had grand illusions of one day working for the great NASA organization. These aspirations were not serious until he graduated from West Plains High School in 2010 already enrolled in an Aerospace Engineering program. Matthew attended Missouri University of Science and Technology, where he graduated Magna cum Laude with a Bachelor of Science degree in Aerospace Engineering plus a minor in Physics in May of 2014. The summer of that year, he finally achieved his dreams by working as an intern at NASA Marshall Space Flight Center in Huntsville. In August of 2014, he returned to Missouri S&T to begin graduate studies, and received a Master of Science in Aerospace Engineering in December of 2016.